# Robust Transmission for Reconfigurable Intelligent Surface Aided Millimeter Wave Vehicular Communications with Statistical CSI

Yuanbin Chen, Ying Wang, *Member, IEEE,* and Lei Jiao, *Senior Member, IEEE*

***Abstract*—The integration of reconfigurable intelligent surface (RIS) into millimeter wave (mmWave) vehicular communications offers the possibility to unleash the potential of future proliferating vehicular applications. However, the high-mobility-induced rapidly varying channel state information (CSI) has been making it challenging to obtain the accurate instantaneous CSI (I-CSI) and to cope with the incurable high signaling overhead. The situation may become worse when the RIS with a large number of passive reflecting elements is deployed. To overcome this challenge, we investigate in this paper a robust transmission scheme for the time-varying RIS-aided mmWave vehicular communications, in which, specifically, a multi-antenna base station (BS) serves vehicle user equipments (VUEs) with the help of RIS at the mmWave frequency. The uplink average achievable rate is maximized relying only upon the imperfect knowledge of statistical CSI. Considering the time-varying characteristics, we first propose an effective transmission protocol by reasonably configuring the time-scale of CSI acquisition in order to significantly relax the frequency of channel information updates, which constitutes one of the most critical issues in RIS-aided vehicular communications. Then, the formulated resource allocation problem is discussed in the single- and multi-VUE case, respectively. To be specific, for the single-VUE case, a closed-form expression of the average rate is derived by extracting the statistical characteristics of mmWave channels, and an alternating optimization (AO)-based algorithm is proposed. For the multi-VUE case, we develop an efficient algorithm, called JAPMC, to circumvent the unavailability of the closed-form of the objective function and probabilistic constraint by constructing quadratic surrogates of that. Simulation results confirm the effectiveness and robustness of our proposed algorithms as compared to benchmark schemes.**

***Index Terms*—Reconfigurable intelligent surface, millimeter wave, vehicular communications, statistical CSI, robust transmission, non-convex stochastic optimization.**

## I. Introduction

Vehicular communications, also known as vehicle-to-everything (V2X) communications, are the key enabler for the autonomous driving, intelligent transportation systems, and on-wheel infotainment services. Nowadays, the two key technologies that support V2X communications are IEEE 802.11p and 3rd Generation Partnership Project (3GPP) Cellular-V2X (C-V2X), which, nevertheless, fall short of satisfying the prospective extreme traffic demands (e.g., in terms of very high throughput, ultra low latency, and ultra high reliability) of future vehicular applications [1] [2]. In this connection, different standardization activities are currently being facilitated by the IEEE and the 3GPP, with the 802.11bd [3] and new radio (NR) V2X [4] specifications, respectively, to surmount the limitations of legacy technologies. Both standards aim at boosting the wireless capacity by encompassing the possibility of using, besides traditional sub-6 GHz frequencies, the lower part of the millimeter-wave (mmWave) spectrum, which features the availability of large chunks of untapped bandwidth. The unique characteristics of mmWave signals, including channel sparsity and high temporal time and angular resolution, can be adopted for precise vehicle positioning, which is very friendly to autonomous driving applications. However, V2X communications at mmWave frequency band remain ongoing challenges [5]: i) communication at mmWave suffers from severe path and penetration losses, and is susceptible to blocking; ii) in high mobility scenarios, the Doppler spread for signal transmission over the mmWave bands tends to be much larger, which becomes a major implementation bottleneck to realize the promising vision of mmWave systems; iii) the exchange of CSI needs to be timely enough to avoid the feedback of stale information in scenarios with a highly varying channel, which, nonetheless, incurs fairly heavy signaling overhead. Faced with these challenges, although intensive research activities are carried out in IEEE and 3GPP, there is still a lack of adequate discussion to overcome such limitations.

Recently, benefitted from the development of advanced radio frequency (RF) and micro-electro-mechanical systems (MEMS), a proposal to integrate reconfigurable intelligent surface (RIS) into wireless communication systems has been introduced [6] [7], especially in vehicular networks [8] [9], which features possibility to customize the wireless propagation environment. Furthermore, RIS can be fabricated as artificial thin films attached to existing infrastructure, such as the facades of buildings, buses and road signs, which greatly reduces the implementation costs. When the line-of-sight (LoS) links are blocked by obstacles, RIS can receive and superimpose multi-path signals from the transmitter, and independently reflect the incident signal by controlling the amplitude and/or phase to achieve passive beamforming. Thus, the resultant "virtual LoS links" can significantly alleviate the blockage effects while improving the transmission performance over mmWave bands. In addition, an RIS-aided MIMO system can achieve the same performance gain as a massive

*Corresponding author: Ying Wang.*

Y. Chen and Y. Wang are with the State Key Laboratory of Networking and Switching Technology, Beijing University of Posts and Telecommunications, Beijing, China 100876 (e-mail: chen_yuanbin@163.com; wangying@bupt.edu.cn). The work of the two authors was supported by the 111 Project of China under Grant B16006.

L. Jiao is with the Department of Information and Communication Technology, University of Agder, N-4879 Grismtad, Norway (e-mail: lei.jiao@uia.no).

MIMO system without RIS, but with significantly reduced active antennas/RF chains [6]. This evinces that a large number of antennas at the BS may not be a requisite anymore, which enables the mmWave systems to be more cost-effective and energy-efficient.

The main design and implementation challenges posed by RIS-aided mmWave communication systems include the requirement of estimating the CSI of associated channels and thereafter the demand of appropriately configuring the RIS reflection coefficients, since the system performance is highly dependent on the accuracy of the obtained CSI and the corresponding RIS configurations. As recently indicated in [10], the overhead caused by the channel estimation and configuration of RIS reflection coefficients may offset the performance gains introduced by an RIS, provided that the magnitude of reflecting elements number is large and/or an inefficient protocol/algorithm is exploited. Furthermore, due to the dynamic behavior of the mobile channel and the mobility of VUEs, it is difficult to track the rapidly varying and easily outdated instantaneous CSI (I-CSI), and frequent feedback of the fast fading information of rapidly varying mobile channels also incurs substantial signaling overhead [11]. An RIS, in this instance, needs to have the capability of reconfiguring itself at an appropriate time-scale that depends on the coherence time of the channel, and the corresponding transmission protocol should also be well-designed.

Motivated by these considerations, there is in general a consensus that it is imperative to consider the increased complexity of transmission strategy in RIS-aided mmWave vehicular communication systems. One of the key factors to be deliberated is the time-scale of CSI acquisition owing to the unavailability of rapidly varying I-CSI. Compared with the I-CSI, the statistical CSI (S-CSI), e.g., the angles of arrival/departure (AoAs/AoDs), and the channel mean, varies more slowly and can be comparatively easily and accurately explored. For this reason, researches on the design of RIS-aided systems by exploiting S-CSI have been investigated in [12]–[15]. To be specific, in [12], an optimization algorithm to effectively configure RISs is proposed, which is aimed at maximizing the network sum-rate by exploiting only the statistical characterization of the environment. The power scaling law analysis and phase shift optimization for an uplink RIS-aided massive multiple-input-multiple-output (MIMO) system based on the S-CSI is investigated in [13]. It is investigated in [14] [15] that a novel two-timescale transmission protocol is proposed for the RIS-aided wireless communication system, where the precoding vector is designed based on the I-CSI and the RIS phase shifts are optimized based on the S-CSI. However, the common denominator of transmission schemes and protocols in [12]–[15] is confined with the quasi-static scenario, which are not suitable for the case of RIS-aided vehicular communications, mainly due to the lack of consideration of Doppler effect originating from the high mobility of vehicles.

Besides the Doppler effect, the accuracy of CSI acquisition is another important aspect to be considered, since the obtained CSI tends to become quickly outdated due to, e.g., mobility. The studies on the scenarios that do not necessarily rely upon the perfect knowledge of the CSI in RIS-aided systems are carried out in [16]–[19], including bounded CSI error model [16] [17] and statistical error model [18] [19]. The former aims to conservatively guarantee the worst case quality-of-service (QoS) constraint while the latter characterizes the practical channel estimation error that is unbounded [20]. Nonetheless, the works in [16]–[19] are still subject to the static scenario, without considering the effects of outdated CSI in time-varying dynamic environment. Distinct from RIS-aided static systems, this property is non-negligible. Thus, the transmission scheme in RIS-aided vehicular communications ought to be robust to the dynamic behaviors of time-varying channels. In a nutshell, we target these non-trivial challenges in this paper to design a robust transmission strategy for the time-varying RIS-aided mmWave vehicular communications.

Against this background, the main contributions of the present work can be summarized as follows:

- We consider a time-varying RIS-aided mmWave vehicular communication system, in which a multi-antenna BS serves uplink transmission with the help of RIS with a plurality of programmable phase shifters. By exploiting the property that AoA/AoDs usually vary much more slowly than complex path gains over mobile channels [21] [22], a novel transmission frame structure is proposed for the time-varying RIS-aided mmWave vehicular communication system. Within a transmission frame composed of a certain number of blocks, the AoA/AoDs of all links are estimated once in the frame header, followed by the complex gain estimation of VUE-related links in each block. Owing to the outdated CSI and unavailability of fast fading information, the transmission design relies only on the imperfect knowledge of the obtained per-block S-CSI.
- We formulate the problem to maximize the uplink average achievable sum-rate by jointly designing active and passive beamforming in each block, subject to the constraints of outage probability and unit-modulus of the RIS phase shifts. This yields a non-convex stochastic optimization problem, which, in particular, is discussed in the single- and multi-VUE case, respectively, in order to draw useful insights.
- For the single-VUE case, it is analyzed that the original stochastic optimization problem can be transformed into a deterministic non-convex optimization problem. By leveraging alternating optimization (AO) approach, the solutions of the multi-user detection (MUD) matrix and the RIS phase shifts are glued together and updated in an iteration manner. Next, a general multi-VUE case is considered. Different from the single-VUE case, it is difficult to derive closed-form expressions of achievable ergodic rates of all VUEs. To circumvent this issue, an effective algorithm, namely JAPMC, that jointly designs active and passive beamforming is proposed under the constrained stochastic successive convex approximation (CSSCA) framework. Particularly, quadratic surrogates of the functions without a closed form are constructed based on certain appropriately generated channel realiza-

tions/samples according to the properties of the considered system and the gradient information of the variables. Hence, a convex surrogate problem is constituted and solved in each iteration to approximate the asymptotic optimal solution.

- Simulation results are presented to substantiate the convergence, effectiveness, and robustness of the proposed algorithms in single-VUE and multi-VUE cases, respectively. Numerical results reveal that the increment of the RIS reflecting elements, especially as the channel conditions deteriorate, does not always give rise to the performance improvement. The extremely high CSI uncertainty will drastically degrade the performance of the RIS-aided system. In addition, the proposed transmission scheme is robust to the performance loss caused by mobility-induced outdated CSI, and retains the average sum-rate at a favorable level even in hostile CSI case.

The remainder of this paper is organized as follows. Section II elaborates the system model and the problem formulation. In Sections III and IV, we propose efficient algorithms to solve the formulated non-convex stochastic optimization problems in the single-VUE and multi-VUE cases, respectively. Simulation results are provided in Section V, and, finally, Section VI concludes the paper.

*Notation:* The following notations and symbols are used throughout this paper. Italic letters denote scalars. Boldface lower- and upper-case letters denote vectors and matrices, respectively. $\mathbb{C}^{M\times N}$ represents the complex space with $M\times N$ dimension, and $\mathbf{I}_N$ denotes an $N\times N$ identity matrix. $\{\cdot\}^*$, $\{\cdot\}^T$, and $\{\cdot\}^H$ stand for the conjugate, transpose, and Hermitian (conjugate transpose) operators, respectively. The symbols $|\cdot|$, $\|\cdot\|$, and $\|\cdot\|_F$ denote the absolute value of a scalar, the $\ell_2$-norm of a vector and the Frobenius norm of a matrix, respectively. $\odot$ and $\otimes$ indicate the Hadamard product and Kronecker product, respectively. $\mathrm{Tr}(\cdot)$, $\mathrm{diag}(\cdot)$, $\mathrm{rank}(\cdot)$ and $\mathrm{egi}(\cdot)$ represent trace, diagonalization, rank and eigenvalue of a square matrix, respectively. $\mathrm{vec}(\cdot)$ is the vectorization operator for a matrix. $\jmath$ is the imaginary unit, i.e., $\jmath^2=-1$. $\Re\{\cdot\}$ and $\Im\{\cdot\}$ denote the real part and the imaginary part of a complex value, respectively. The distribution of a circularly symmetric complex Gaussian (CSCG) with zero mean and variance $\Sigma$ is denoted by $\mathcal{CN}(0,\Sigma)$. $\sim$ stands for "distributed as". $\mathbb{E}\{\cdot\}$ represents the statistical expectation operator. $\chi^2(\upsilon)$ denotes a chi-square random variable with degree of freedom $\upsilon$. For two given sets $\mathcal{A}$ and $\mathcal{B}$, $\mathcal{A}\backslash\mathcal{B}\triangleq\{x|x\in\mathcal{A},x\notin\mathcal{B}\}$.

## II. System Model and Problem Formulation

### A. Scenario

As shown in Fig. 1, we consider an RIS-aided uplink multiple-input-single-output (MISO) mmWave vehicular communication system, in which the BS is equipped with a $K$-element uniform linear array (ULA) and the VUEs, the set of which is denoted by $\mathcal{M}=\{1,2,...,M\}$, are equipped with a single antenna. The VUEs communicate with the BS through vehicle-to-infrastructure (V2I) links. The RIS is a uniform rectangular array (URA) composed of $N_\mathrm{h}$ horizontally arranged and $N_\mathrm{v}$ vertically arranged passive reflecting

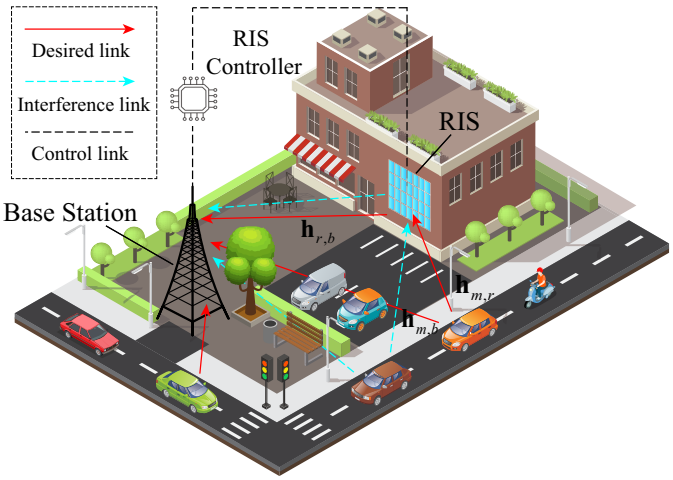


Fig. 1. Reconfigurable intelligent surface aided vehicular communications.

elements. Thus the total number of RIS reflecting elements is $N{=}N_\mathrm{h}\times N_\mathrm{v}$. In the considered system, the RIS reflection coefficients are coordinated by the BS and then sent back to the RIS controller via a separate backhaul link. For simplicity, it is assumed that the amplitude reflection coefficients are set to one for all reflecting elements to maximize the signal reflection [16] [17], and denote the phase reflection coefficient of the $n$th reflecting element by $\theta_n=e^{\jmath\varphi_n}$, where $\varphi_n\in[0,2\pi)$. More practical RIS reflection coefficients such as low-resolution discrete phases shifts are to be discussed and evaluated in Sec. V. B later. Then, the RIS reflection-coefficient matrix is defined as $\mathbf{\Theta}=\mathrm{diag}(\theta_1,...,\theta_N)$, which is an $N\times N$ diagonal matrix, also known as the passive beamforming matrix [14].

### B. Time-varying mmWave Channel Model and Communication Protocol

The mmWave channel model is specified when the Doppler effect is considered. Herein we adopt the time-varying 3D Saleh-Valenzuela channel model [21] with $L_{m,b}$, $L_{m,r}$ and $L_{r,b}$ propagation paths for the BS-VUE links, the RIS-VUE links and the BS-RIS links, respectively. A transmission frame composed of $T$ blocks is considered in our model, where $\mathcal{T}=\{1,...,T\}$. Accordingly, the channel gain from the $m$th VUE to the BS and the channel gain from the $m$th VUE to the RIS in the $t$th block are denoted by

$$\mathbf{h}_{m,b}[t]=\sqrt{\frac{1}{L_{m,b}}}\sum_{l=1}^{L_{m,b}}\beta_{m,b,l}^{t}\mathbf{a}_L\left(\vartheta_{m,b,l}^{\mathrm{AoA}}\right),\forall m,t, \quad (1)$$

$$\mathbf{h}_{m,r}[t]=\sqrt{\frac{1}{L_{m,r}}}\sum_{l=1}^{L_{m,r}}\beta_{m,r,l}^{t}\mathbf{a}_P\left(\vartheta_{m,r,l}^{\mathrm{AoA}},\phi_{m,r,l}^{\mathrm{AoA}}\right),\forall m,t. \quad (2)$$

Since the BS and the RIS are placed in fixed positions, the BS-RIS channel is quasi-static that can be denoted by

$$\mathbf{h}_{r,b}=\sqrt{\frac{1}{L_{r,b}}}\sum_{l=1}^{L_{r,b}}h_{r,b,l}\mathbf{a}_L\left(\vartheta_{r,b,l}^{\mathrm{AoA}}\right)\mathbf{a}_P^H\left(\vartheta_{r,b,l}^{\mathrm{AoD}},\phi_{r,b,l}^{\mathrm{AoD}}\right). \quad (3)$$

In (1)–(3), $l=1$ denotes the LoS paths, and $l\geq 2$ denotes the non-line-of-sight (NLoS) paths. $\beta_{m,b,l}^{t}=h_{m,b,l}e^{\jmath 2\pi f_{m,b,l}tT_s}$

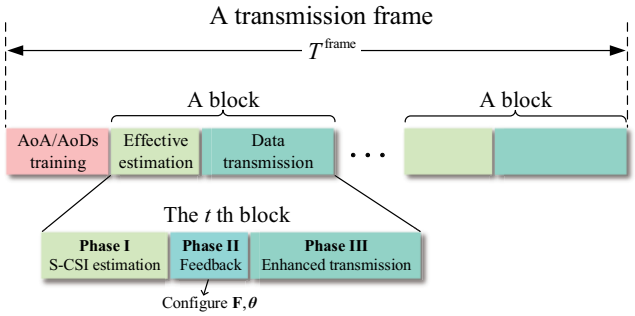


Fig. 2. The proposed transmission protocol.

and $\beta_{m,r,l}^{t} = h_{m,r,l} e^{\jmath 2\pi f_{m,r,l} t T_s}$ denote the time-varying complex gains incorporating the Doppler shifts $\{f_{m,b,l}, f_{m,r,l}\}$, respectively, which vary independently from one block to another in the considered transmission frame, and $T_s$ represents the system sampling period. The large-scale fading coefficients are defined as $h \in \{h_{m,b,l}, h_{m,r,l}, h_{r,b,l}\}$, following a complex Gaussian distribution as $h \sim \mathcal{CN}\left(0, 10^{-0.1\text{PL}}\right)$, where $\text{PL}\,(\text{dB}) = \text{PL}_0 + 10\alpha \lg(D) + \text{PL}_s$, $\text{PL}_0$ is the path loss at the reference distance of one meter, $D$ (in meters) represents the individual link distance, $\alpha$ denotes the path-loss exponent, and $\text{PL}_s \sim \mathcal{CN}\left(0, \sigma_s^2\right)$ is the shadow fading following complex Gaussian distribution with zero mean and variance $\sigma_s^2$. The steering vector of the ULA is denoted by $\mathbf{a}_L(\vartheta) = \left[1, e^{\jmath 2\pi \frac{d}{\lambda} \sin\vartheta}, ..., e^{\jmath 2\pi \frac{d}{\lambda}(K-1)\sin\vartheta}\right]^T$, where $\vartheta$ stands for the azimuth AoAs $\vartheta_{m,b,l}^{\text{AoA}}$ and $\vartheta_{r,b,l}^{\text{AoA}}$, $d$ is the antenna inter-spacing , and $\lambda$ is the carrier wavelength. The steering vector of the URA can be expressed as $\mathbf{a}_P(\vartheta, \phi) = \mathbf{a}_L(\vartheta) \otimes \mathbf{a}_L(\phi)$, where $\vartheta(\phi)$ is the azimuth (elevation) AoD $\vartheta_{r,b,l}^{\text{AoD}}\left(\phi_{r,b,l}^{\text{AoD}}\right)$ and the AoA $\vartheta_{m,r,l}^{\text{AoA}}\left(\phi_{m,r,l}^{\text{AoA}}\right)$.

It is worthy mentioning that high mobility in a vehicular environment precludes the collection of the accurate full I-CSI at the BS. Frequent feedback of the fast fading information leads to a mass of signaling overhead, which cannot be realized by tracking I-CSI of rapidly varying mobile channels in practice. Thus, we assume in this paper that the BS can only access per-block statistical fading information (S-CSI) of such channels instead of each realization of the I-CSI. More explicitly, since the AoA/AoDs and complex gains vary slowly in a high-mobility scenario, it is reasonable to make the same assumption presented in [21] that the AoA/AoDs $\vartheta(\phi)$, which are typically determined by the locations of vehicles, remain constant during the considered frame. Thus, the time-varying channel model in the RIS-aided mmWave system only concerns the effect of Doppler shifts subject to the changes from one block to another. Fig. 2 illustrates our proposed transmission protocol for the time-varying mmWave vehicular communications. In particular, a frame with time duration $T^{\text{frame}}$ consists of one phase of AoA/AoDs estimation, followed by a certain amount blocks. In each block, the acquisition and the utilization of the S-CSI is divided into three phases. In the first phase, the RIS is in the sensing mode and the channel statistical information between the RIS and the BS/VUEs can be estimated by resorting to the dedicated sensors at the RIS and leveraging the pilots and/or data transmitted in both uplink and downlink. Since the channel estimation is out of the scope of this paper, we do not expand the discussion here. One can find from [20] [23] the research studies on how to estimate the channels for RIS-aided systems. In the second phase, based on the measured per-block S-CSI of the BS-RIS-VUE links that fed by the RIS and that of the BS-VUE link, the BS computes the active and the passive beamforming matrices, and sends them to the RIS through the dedicated backhaul link to enhance the transmission in the third phase.

Let the MUD matrix (also known as the combining matrix) be $\mathbf{F} = [\mathbf{f}_1, ..., \mathbf{f}_M] \in \mathbb{C}^{K\times M}$, and $\mathbf{f}_m \in \mathbb{C}^{K\times 1}$ is the $m$th column of the matrix $\mathbf{F}$. The received signal at the BS from the $m$th VUE at the $t$th block can be formulated as

$$y_m[t] = \mathbf{f}_m^H \left(\sqrt{P_m}\left(\mathbf{h}_{r,b}\boldsymbol{\Theta}\mathbf{h}_{m,r}[t] + \mathbf{h}_{m,b}[t]\right) s_m[t] + \boldsymbol{n}_m[t]\right), \tag{4}$$

where $s_m[t]$ and $P_m$ represent the transmitted information symbol and the transmit power of the $m$th VUE, respectively. The noise vector is denoted by $\boldsymbol{n}_m[t] \in \mathbb{C}^{K\times 1}$, and it is assumed that $\boldsymbol{n}_m[t] \sim \mathcal{CN}\left(\mathbf{0}, \sigma^2\mathbf{I}\right)$. The cascaded channel from the $m$th VUE to the BS at the $t$th block is denoted by $\mathbf{h}_m[t] = \text{diag}\left(\mathbf{h}_{m,r}[t]\right)\mathbf{h}_{r,b}^H \in \mathbb{C}^{N\times K}$. Let $\boldsymbol{\theta} = [\theta_1, ..., \theta_N]^T \in \mathbb{C}^{N\times 1}$ be the vector containing elements in diagonal matrix $\boldsymbol{\Theta}$. Then, the uplink signal-to-interference-plus-noise ratio (SINR) of the $m$th VUE at the $t$th block can be given by

$$\text{SINR}_m[t] = \frac{P_m\left|\mathbf{f}_m^H\left(\mathbf{h}_m^H[t]\,\boldsymbol{\theta} + \mathbf{h}_{m,b}[t]\right)\right|^2}{\sum\limits_{m'\in\mathcal{M}\setminus m} P_{m'}\left|\mathbf{f}_m^H\left(\mathbf{h}_{m'}^H[t]\,\boldsymbol{\theta} + \mathbf{h}_{m',b}[t]\right)\right|^2 + \sigma^2|\mathbf{f}_m^H|^2}. \tag{5}$$

### C. CSI Error Model

Due to the transmission and processing delay, the CSI may be easily stale at the time when the RIS and the VUEs receive the pilots/data from the BS, which results in an inevitable performance loss once this outdated CSI is employed for beamforming. In this case, the temporal correlation coefficient $\rho(T_s)$ is introduced to bridge the real CSI with the outdated CSI according to the Jakes' model [24] [25], i.e., $\rho(T_s) = J_0(2\pi f_{\max} T_s)$, where $J_0$ represents the zeroth-order Bessel function of the first kind, and $f_{\max}$ denotes the maximum Doppler shift. Thus, the evolution of the uncertain direct channel $\mathbf{h}_{m,b}[t]$ over the time can be characterized approximately by leveraging the first-order autoregressive model [22] [26], which is given by

$$\mathbf{h}_{m,b}[t] = \rho_{m,b}(T_s)\,\hat{\mathbf{h}}_{m,b}[t - T_s] + \Delta\mathbf{h}_{m,b}[t], \forall m, t, \tag{6}$$

where $\hat{\mathbf{h}}_{m,b}[t - T_s]$ is the estimated CSI, and $\Delta\mathbf{h}_{m,b}$ is the unknown residual error that follows $\Delta\mathbf{h}_{m,b}[t] \sim \mathcal{CN}\left(\mathbf{0}, \left(1 - \rho_{m,b}(T_s)^2\right)\boldsymbol{\Sigma}_m^d\right), \boldsymbol{\Sigma}_m^d \succeq \mathbf{0}, \forall m \in \mathcal{M}, t \in \mathcal{T}$. Along the same line, the evolution of the uncertain cascaded channel $\mathbf{h}_m[t]$ can be expressed by

$$\mathbf{h}_m[t] = \rho_m(T_s)\,\hat{\mathbf{h}}_m[t - T_s] + \Delta\mathbf{h}_m[t], \forall m, t, \tag{7}$$

where $\hat{\mathbf{h}}_m[t-T_s]$ is the estimated cascaded CSI, and the error term $\Delta\mathbf{h}_m[t]$ follows $\Delta\mathbf{h}_m[t] \sim \mathcal{CN}\left(\mathbf{0}, \left(1-\rho_m(T_s)^2\right)\boldsymbol{\Sigma}_m^c\right), \boldsymbol{\Sigma}_m^c \succeq \mathbf{0}, \forall m \in \mathcal{M}, t \in \mathcal{T}$. $\boldsymbol{\Sigma}_m^d \in \mathbb{C}^{K\times K}$ and $\boldsymbol{\Sigma}_m^c \in \mathbb{C}^{NK\times NK}$ are positive semidefinite error covariance matrices. The superscript "$d$" means "direct" and the superscript "$c$" signifies "cascaded". For the convenience of subsequent derivation, some definitions are given: $\boldsymbol{\Sigma}_m^c = (\eta_m^c)^2\mathbf{I}$, $\mathrm{vec}(\Delta\mathbf{h}_m) = \eta_m^c\mathbf{i}_m^c$, $\mathbf{i}_m^c \in \mathbb{C}^{NK\times 1} \sim \mathcal{CN}(\mathbf{0},\mathbf{I})$; $\boldsymbol{\Sigma}_m^d = \left(\eta_m^d\right)^2\mathbf{I}$, $\Delta\mathbf{h}_{m,b} = \eta_m^d\mathbf{i}_m^d$, and $\mathbf{i}_m^d \in \mathbb{C}^{K\times 1} \sim \mathcal{CN}(\mathbf{0},\mathbf{I})$.

The CSI imperfection mainly stems from the channel estimation as the conventional minimum mean-squared error (MMSE) method is generally employed to estimate the cascaded channel [27], which endows the uncertain residual errors, e.g., $\Delta\mathbf{h}_{m,b}[t]$ and $\Delta\mathbf{h}_m[t]$, with stochastic nature to follow complex Gaussian distributions. Thus, the error models in (6) and (7) belong to the statistical CSI error model in essence. Compared with the bounded error model that is usually employed to portray the channel quantization errors, the temporal correlative error model captures the property of the high-mobility-induced outdated CSI and is more practical in a time-varying environment with abundant scatters. Thus, the to-be-designed robust transmission is based on such a model with statistical CSI error subject to the outage probability, which is more suitable for our case to appropriately characterize the outdated channel estimation error.

### D. Problem Formulation

In this paper, we aim to maximize the uplink average achievable sum-rate in each block by jointly optimizing the transmit power $\mathbf{P} = \{P_m, \forall m\}$, the MUD matrix $\mathbf{F}$ at the BS and the RIS reflection phase shifts $\boldsymbol{\theta}$, subject to the unit-modulus and the outage probability constraints, i.e., ensuring the probability that the per-block SINR of each VUE is less than a threshold under the channel error realizations being below a predetermined value. Thus, the optimization problem of the robust transmission for the RIS-aided mmWave vehicular communications can be formulated as follows

$$\max_{\{\mathbf{P},\boldsymbol{\theta},\mathbf{F}\}} \quad \mathbb{E}\left[\frac{1}{T}\sum_{t\in\mathcal{T}}\sum_{m\in\mathcal{M}}\log_2\left(1+\mathrm{SINR}_m[t]\right)\right] \tag{8a}$$

$$s.t. \quad \Pr\left(\mathrm{SINR}_m[t] \le \gamma^{\mathrm{th}}\right) \le p_0, \forall m, t, \tag{8b}$$

$$|\theta_n| = 1, \forall n, \tag{8c}$$

$$0 \le P_m \le P_{\max}, \forall m, \tag{8d}$$

where (8b) ensures the probability that the per-block decoding error of each VUE at a certain SINR, $\mathrm{SINR}_m[t]$, is less than the maximum tolerable outage probability $p_0$, $\gamma^{\mathrm{th}}$ is the SINR threshold, and (8d) confines the maximum transmit power of each VUE.

Although the joint design of the active and passive beamforming is adjusted with the per-block CSI, the AoA/AoDs of each channel are estimated and remain fixed in the transmission frame of the interest, which avoids a mass of pilot/training symbols compared with estimating the high-dimension AoA/AoDs of $\mathbf{h}_{m,b}[t]$ and $\mathbf{h}_{m,b}[t]$ in each block. Now, fewer pilots are needed to probe the low-dimension Doppler shifts. To be specific, the number of channel coefficients (AoA/AoDs) required in each frame can be reduced compared with the case that the statistical information is not exploited, from $T(NK+K+N)$ to $NK+K+N$ for each VUE.

Problem (8) is challenging to solve mainly for the following three reasons: i) the optimization variables, such as the MUD matrix $\mathbf{F}$ and the RIS reflection phase shifts $\boldsymbol{\theta}$, are highly coupled with each other; ii) there is no closed-form expression for the objective function and the constraint in (8b), which exacerbates the difficulty of solving problem (8); iii) it is a non-convex stochastic problem even for $M=1$. Furthermore, there is no efficient method for solving the formulated non-convex stochastic problem (8) optimally. In the next two sections, we propose two effective algorithms to solve problem (8) sub-optimally in the single-VUE and multi-VUE cases, respectively.

## III. Single-VUE Case

This section mainly considers the single-VUE case, i.e., $M=1$, where there is no interference from other VUEs. Accordingly, problem (8) reduces to

$$\max_{\{\mathbf{P},\boldsymbol{\theta},\mathbf{F}\}} \mathbb{E}\left[\frac{1}{T}\sum_{t\in\mathcal{T}}\sum_{m\in\mathcal{M}}\log_2\left(1+\frac{P_m\left|\mathbf{f}_m^H\left(\mathbf{h}_m^H[t]\,\boldsymbol{\theta}+\mathbf{h}_{m,b}[t]\right)\right|^2}{\sigma^2\left|\mathbf{f}_m^H\right|^2}\right)\right] \tag{9a}$$

$$s.t. \quad \Pr\left(\frac{P_m\left|\mathbf{f}_m^H\left(\mathbf{h}_m^H[t]\,\boldsymbol{\theta}+\mathbf{h}_{m,b}[t]\right)\right|^2}{\sigma^2\left|\mathbf{f}_m^H\right|^2} \le \gamma^{\mathrm{th}}\right) \le p_0, \forall m, t, \tag{9b}$$

$$(8c), (8d). \tag{9c}$$

For the problem at hand, there are no closed-form expressions for (9a) and (9b). Hence, in the following, we first derive the closed-form expression of the objective function in conformity with the statistical characteristics of the time-varying mmWave channel. Then, the outage constraint in (9b) is transformed according to the Bernstein-type inequality to make it a deterministic optimization problem. The AO method is utilized to obtain a near optimal solution in an iterative manner. For the subsequent analysis, we focus on the per-block uplink achievable rate and outage probability. Thus, the index "$t$" denoting the $t$th block is omitted for simplicity.

### A. Uplink Average Achievable Rate

For any given phase-shift vector $\boldsymbol{\theta}$, it is well-known that the maximum-ratio combining (MRC) at the BS is optimal [28], i.e.,

$$\mathbf{f}_m^{\mathrm{opt}} = \frac{\hat{\mathbf{h}}_m^H\boldsymbol{\theta}+\hat{\mathbf{h}}_{m,b}}{\left\|\hat{\mathbf{h}}_m^H\boldsymbol{\theta}+\hat{\mathbf{h}}_{m,b}\right\|}. \tag{10}$$

Based on the optimal MUD matrix, we have the following proposition.

***Proposition 1:*** In the single-VUE case, the average achievable rate in (9) is upper-bounded by (11), where $\mathbf{A}_m = \sum_{i=1}^{L_{r,b}}\sum_{j=1}^{L_{m,r}}\mathrm{diag}\left(\mathbf{A}_{m,r,j}\right)\mathbf{A}_{r,b,i}^H \in \mathbb{C}^{N\times K}$, $\mathbf{A}_{m,r,j} =$

$$\bar{R}_m^{ub} = \log_2\left[1+\frac{P_m}{\sigma^2}\left(\varpi_m\left\|\hat{\mathbf{A}}_m^H\boldsymbol{\theta}\right\|^2 10^{-0.1(\mathrm{PL}_{m,r}+\mathrm{PL}_{r,b})}+\varpi_{m,b}\left\|\hat{\mathbf{A}}_{m,b}\right\|^2 10^{-0.1\mathrm{PL}_{m,b}}\right.\right.$$
$$\left.\left.+NK\left(\left(\eta_m^c\sqrt{1-\rho_m^2}\right)^2+\left(\eta_m^d\sqrt{1-\rho_{m,b}^2}\right)^2\right)\right)\right]. \tag{11}$$

$$\boldsymbol{\Lambda}_m=\begin{bmatrix}\left(\eta_m^c\sqrt{1-\rho_m^2}\right)^2(\mathbf{I}_K\otimes\boldsymbol{\Theta}) & \eta_m^c\eta_m^d\sqrt{\left(1-\rho_m^2\right)\left(1-\rho_{m,b}^2\right)}(\mathbf{I}_K\otimes\boldsymbol{\theta}^*)\\ \eta_m^c\eta_m^d\sqrt{\left(1-\rho_m^2\right)\left(1-\rho_{m,b}^2\right)}(\mathbf{I}_K\otimes\boldsymbol{\theta}^T) & \left(\eta_m^d\sqrt{1-\rho_{m,b}^2}\right)^2\mathbf{I}_K\end{bmatrix}.$$

$\mathbf{a}_P\left(\vartheta_{m,r,j}^{\mathrm{AoA}},\phi_{m,r,j}^{\mathrm{AoA}}\right)\in\mathbb{C}^{N\times 1},\forall m,j$, $\mathbf{A}_{r,b,i}=\mathbf{a}_L\left(\vartheta_{r,b,i}^{\mathrm{AoA}}\right)\times\mathbf{a}_P^H\left(\vartheta_{r,b,l}^{\mathrm{AoD}},\phi_{r,b,i}^{\mathrm{AoD}}\right)\in\mathbb{C}^{K\times N},\forall i$, $\hat{\mathbf{A}}_{m,b}=\sum_{l=1}^{L_{m,b}}\hat{\mathbf{A}}_{m,b,l}\in\mathbb{C}^{K\times 1}$, $\varpi_m=\frac{\rho_m^2}{L_{r,b}L_{m,r}}\left(\sum_{j=1}^{L_{m,r}}\exp\{\jmath 2\pi f_{m,r,j}tT_s\}\right)^2$, $\varpi_{m,b}=\frac{\rho_{m,b}^2}{L_{m,b}}\left(\sum_{l=1}^{L_{m,b}}\exp\{\jmath 2\pi f_{m,b,l}tT_s\}\right)^2$, and $\hat{\mathbf{A}}$ is the estimation of $\mathbf{A}$.

*Proof:* See Appendix A. ■

In somewhat simplistic, but plausible terms one could argue that the derived upper bound is a tight approximation of the average achievable rate for a single VUE. Due to the unit-modulus constraints in (8c) and the finite matrix eigenvalues of the quadratic form, i.e., $\left\|\hat{\mathbf{A}}_m^H\boldsymbol{\theta}\right\|^2$ and $\left\|\hat{\mathbf{A}}_{m,b}\right\|^2$ in (11), there will be no unbounded situation even if maximizing the upper bound of the average achievable rate, as verified in [14]. Based on Proposition 1, the $\log_2(\cdot)$ operator can be removed in the logarithmic rate upper-bound function due to its monotonicity. Some coefficients and constant terms can also be ignored. Problem (9) can then be transformed to the following problem

$$\max_{\{\mathbf{P},\boldsymbol{\theta}\}}\quad P_m\left\|\hat{\mathbf{A}}_m^H\boldsymbol{\theta}\right\|^2 \tag{12a}$$
$$s.t.\quad \Pr\left(P_m\left\|\mathbf{h}_m^H\boldsymbol{\theta}+\mathbf{h}_{m,b}\right\|^2\le\sigma^2\gamma^{\mathrm{th}}\right)\le p_0,\forall m, \tag{12b}$$
$$(8\mathrm{c}),(8\mathrm{d}). \tag{12c}$$

### *B. Outage Constrained CSI Error Model*

The outage constrained robust transmission problem in (12) is computationally intractable due to the fact that the outage probability constraint (12b) has no simple closed-form expressions. To tackle this issue, a safe approximation based on Bernstein-type inequality [29, Lemma 1] [19] is employed. First, let us reformulate the outage probability in (12b) by using the following proposition.

***Proposition 2:*** The outage probability constraint in (12b) can be converted to

$$\Pr\left(\mathbf{i}_m^H\boldsymbol{\Lambda}_m\mathbf{i}_m+2\Re\left\{\mathbf{v}_m^H\mathbf{i}_m\right\}+v_m\ge 0\right)\ge 1-p_0,\forall m, \tag{13}$$

where $\boldsymbol{\Lambda}_m$ is given at the top of this page, $\mathbf{v}_m=\begin{bmatrix}\eta_m^c\sqrt{1-\rho_m^2}\mathrm{vec}^*\left(\boldsymbol{\theta}\left(\rho_m\boldsymbol{\theta}^H\hat{\mathbf{h}}_m+\rho_{m,b}\hat{\mathbf{h}}_{m,b}^H\right)\right)\\ \eta_m^d\sqrt{1-\rho_{m,b}^2}\left(\rho_m\hat{\mathbf{h}}_m^H\boldsymbol{\theta}+\rho_{m,b}\hat{\mathbf{h}}_{m,b}\right)\end{bmatrix}$, and $v_m=\left(\rho_m\boldsymbol{\theta}^H\hat{\mathbf{h}}_m+\rho_{m,b}\hat{\mathbf{h}}_{m,b}^H\right)\left(\rho_m\hat{\mathbf{h}}_m^H\boldsymbol{\theta}+\rho_{m,b}\hat{\mathbf{h}}_{m,b}\right)-\sigma^2\gamma^{\mathrm{th}}/P_m$.

*Proof:* See Appendix B. ■

According to Lemma 1 in [29], by introducing slack variables $\tilde{\mathbf{x}}=[\tilde{x}_1,...,\tilde{x}_M]^T\in\mathbb{C}^{M\times 1}$ and $\tilde{\mathbf{y}}=[\tilde{y}_1,...,\tilde{y}_M]^T\in\mathbb{C}^{M\times 1}$, (13) can be converted into

$$\begin{cases}\mathrm{Tr}\{\boldsymbol{\Lambda}_m\}-\sqrt{2\ln(1/p_0)}\tilde{x}_m+\ln(p_0)\,\tilde{y}_m+v_m\ge 0\\ \sqrt{\|\boldsymbol{\Lambda}_m\|_F^2+2\|\mathbf{v}_m\|^2}\le\tilde{x}_m\\ \tilde{y}_m\mathbf{I}+\boldsymbol{\Lambda}_m\succeq\mathbf{0},\tilde{y}_m\ge 0\end{cases}, \tag{14}$$

Then, some complex terms in (14) can be simplified as given in (15) at the top of the next page, where (a) holds due to [30, in P421]. Thus we obtain

$$\begin{aligned}&\tilde{y}_m\mathbf{I}_K+\boldsymbol{\Lambda}_m\succeq\mathbf{0}\\ \Rightarrow&\tilde{y}_m\mathbf{I}_K+\left[\left(\eta_m^c\sqrt{1-\rho_m^2}\right)^2N+\left(\eta_m^d\sqrt{1-\rho_{m,b}^2}\right)^2\right]\mathbf{I}_K\succeq\mathbf{0}.\end{aligned} \tag{16}$$

Combined with the above analysis, problem (12) is approximated as the problem shown in (17) at the next page. Although problem (17) is simplified to a certain extent compared to problem (9), it is still non-convex and is difficult to solve, dominantly resulting from the coupled variables $\mathbf{P}$ and $\boldsymbol{\theta}$. In the following analysis, AO is employed to decouple such variables. Specifically, for any given reflection phase shifts $\boldsymbol{\theta}$ at the RIS, the transmit power $\mathbf{P}$ can be optimized by solving a convex problem. Then, for any given $\mathbf{P}$, the RIS reflection phase shifts $\boldsymbol{\theta}$ can be efficiently designed by leveraging the penalty CCP method due to the non-convexity of the decomposed subproblem.

### *C. AO for Solving Problem (17)*

*1) Optimization of Transmit Power:* For the fixed RIS reflection phase shifts $\boldsymbol{\theta}$, the problem optimizing the transmit power of each VUE can be formulated as follows

$$\max_{\{\mathbf{P},\tilde{\mathbf{x}},\tilde{\mathbf{y}}\}}\quad P_m\left\|\hat{\mathbf{A}}_m^H\boldsymbol{\theta}\right\|^2 \tag{18a}$$
$$s.t.\quad (8\mathrm{d}),(17\mathrm{c})-(17\mathrm{e}). \tag{18b}$$

$$\begin{aligned}\mathrm{Tr}\left\{\mathbf{\Lambda}_m\right\} =&\mathrm{Tr}\left\{\left[\begin{array}{c}\eta_m^c\sqrt{1-\rho_m^2}\left(\mathbf{I}_K\otimes\boldsymbol{\theta}^*\right)\\ \eta_m^d\sqrt{1-\rho_{m,b}^2}\mathbf{I}_K\end{array}\right]\cdot\left[\begin{array}{cc}\eta_m^c\sqrt{1-\rho_m^2}\left(\mathbf{I}_K\otimes\boldsymbol{\theta}^T\right) & \eta_m^d\sqrt{1-\rho_{m,b}^2}\mathbf{I}_K\end{array}\right]\right\}\\ =&\mathrm{Tr}\left\{\left(\eta_m^c\sqrt{1-\rho_m^2}\right)^2\left(\mathbf{I}_K\otimes\mathbf{\Theta}\right)+\left(\eta_m^d\sqrt{1-\rho_{m,b}^2}\right)^2\mathbf{I}_K\right\}\\ =&\left(\eta_m^c\sqrt{1-\rho_m^2}\right)^2NK+\left(\eta_m^d\sqrt{1-\rho_{m,b}^2}\right)^2K, \end{aligned}\tag{15a}$$

$$\left\|\mathbf{\Lambda}_m\right\|_F^2=\mathrm{Tr}\left\{\mathbf{\Lambda}_m\mathbf{\Lambda}_m^H\right\}=\left[\left(\eta_m^c\sqrt{1-\rho_m^2}\right)^2N+\left(\eta_m^c\sqrt{1-\rho_{m,b}^2}\right)^2\right]^2,\tag{15b}$$

$$\begin{aligned}\left\|\mathbf{v}_m\right\|^2=&\left[\begin{array}{cc}\eta_m^c\sqrt{1-\rho_m^2}\mathrm{vec}^T\left(\boldsymbol{\theta}\left(\rho_m\boldsymbol{\theta}^H\hat{\mathbf{h}}_m+\rho_{m,b}\hat{\mathbf{h}}_{m,b}\right)\right) & \eta_m^d\sqrt{1-\rho_{m,b}^2}\left(\rho_m\boldsymbol{\theta}^H\hat{\mathbf{h}}_m+\rho_{m,b}\hat{\mathbf{h}}_{m,b}^H\right)\end{array}\right]\\ &\times\left[\begin{array}{c}\eta_m^c\sqrt{1-\rho_m^2}\mathrm{vec}^*\left(\boldsymbol{\theta}\left(\rho_m\boldsymbol{\theta}^H\hat{\mathbf{h}}_m+\rho_{m,b}\hat{\mathbf{h}}_{m,b}\right)\right)\\ \eta_m^d\sqrt{1-\rho_{m,b}^2}\left(\rho_m\hat{\mathbf{h}}_m^H\boldsymbol{\theta}+\rho_{m,b}\hat{\mathbf{h}}_{m,b}\right)\end{array}\right]\\ =&\left[\left(\eta_m^c\sqrt{1-\rho_m^2}\right)^2N+\left(\eta_m^d\sqrt{1-\rho_{m,b}^2}\right)^2\right]\left\|\rho_m\boldsymbol{\theta}^H\hat{\mathbf{h}}_m+\rho_{m,b}\hat{\mathbf{h}}_{m,b}^H\right\|_2^2,\end{aligned}\tag{15c}$$

$$\begin{aligned}\mathrm{egi}\left(\mathbf{\Lambda}_m\right)=&\mathrm{egi}\left\{\left[\begin{array}{c}\eta_m^c\sqrt{1-\rho_m^2}\left(\mathbf{I}_K\otimes\boldsymbol{\theta}^*\right)\\ \eta_m^d\sqrt{1-\rho_{m,b}^2}\mathbf{I}_K\end{array}\right]\cdot\left[\begin{array}{cc}\eta_m^c\sqrt{1-\rho_m^2}\left(\mathbf{I}_K\otimes\boldsymbol{\theta}^T\right) & \eta_m^d\sqrt{1-\rho_{m,b}^2}\mathbf{I}_K\end{array}\right]\right\}\\ \overset{(a)}{=}&\mathrm{egi}\left\{\left(\left(\eta_m^c\sqrt{1-\rho_m^2}\right)^2N+\left(\eta_m^d\sqrt{1-\rho_{m,b}^2}\right)^2\right)\mathbf{I}_K\right\},\end{aligned}\tag{15d}$$

---

$$\max_{\{\mathbf{P},\boldsymbol{\theta},\tilde{\mathbf{x}},\tilde{\mathbf{y}}\}}\quad P_m\left\|\hat{\mathbf{A}}_m^H\boldsymbol{\theta}\right\|^2\tag{17a}$$

$$s.t.\quad (8\mathrm{c}),(8\mathrm{d}),\tag{17b}$$

$$\left(\eta_m^c\sqrt{1-\rho_m^2}\right)^2NK+\left(\eta_m^d\sqrt{1-\rho_{m,b}^2}\right)^2K-\sqrt{2\ln\left(1/p_0\right)}\tilde{x}_m+\ln\left(p_0\right)\tilde{y}_m+v_m\geq 0,\forall m,\tag{17c}$$

$$\left\|\begin{array}{c}\left(\left(\eta_m^c\sqrt{1-\rho_m^2}\right)^2NK+\left(\eta_m^d\sqrt{1-\rho_{m,b}^2}\right)^2K\right)\mathrm{vec}\left(\mathbf{I}_K\right)\\ \sqrt{2\left(\left(\eta_m^c\sqrt{1-\rho_m^2}\right)^2N+\left(\eta_m^d\sqrt{1-\rho_{m,b}^2}\right)^2\right)}\left(\rho_m\hat{\mathbf{h}}_m^H\boldsymbol{\theta}+\rho_{m,b}\hat{\mathbf{h}}_{m,b}\right)\end{array}\right\|\leq\tilde{x}_m,\forall m,\tag{17d}$$

$$\tilde{y}_m\mathbf{I}_K+\left[\left(\eta_m^c\sqrt{1-\rho_m^2}\right)^2N+\left(\eta_m^d\sqrt{1-\rho_{m,b}^2}\right)^2\right]\mathbf{I}_K\succeq\mathbf{0},\forall m.\tag{17e}$$

---

Problem (18) is convex and can be efficiently solved by the existing solver, such as CVX [31].

*2) Optimization of RIS Reflection Phase Shifts:* For any given transmit power $\mathbf{P}$, the RIS reflection phase shifts can be designed by solving the following problem

$$\max_{\{\boldsymbol{\theta},\tilde{\mathbf{x}},\tilde{\mathbf{y}}\}}\quad P_m\left\|\hat{\mathbf{A}}_m^H\boldsymbol{\theta}\right\|^2\tag{19a}$$

$$s.t.\quad (8\mathrm{c}),(17\mathrm{c})-(17\mathrm{e}).\tag{19b}$$

The non-concavity of the objective function and the non-convex constraints (8c), (17c) endow this subproblem with intractability. To solve problem (19) effectively and efficiently, we resort to the penalty CCP [17] [32] method to deal with the non-convex terms. Following the penalty CCP, the objective function is lower bounded by its first order Taylor expansion at the given point $\boldsymbol{\theta}^{(q)}$ in the $q$th iteration, which is given by $\boldsymbol{\theta}^H\hat{\mathbf{A}}_m\hat{\mathbf{A}}_m^H\boldsymbol{\theta}\geq 2\Re\left\{\left(\boldsymbol{\theta}^H\right)^{(q)}\hat{\mathbf{A}}_m\hat{\mathbf{A}}_m^H\boldsymbol{\theta}\right\}-\left(\boldsymbol{\theta}^H\right)^{(q)}\hat{\mathbf{A}}_m\hat{\mathbf{A}}_m^H\boldsymbol{\theta}^{(q)}$. The term $\boldsymbol{\theta}^H\hat{\mathbf{h}}_m\hat{\mathbf{h}}_m^H\boldsymbol{\theta}$ involved in $v_m$ leads to the non-convexity of (17c). Similarly, at the given point $\boldsymbol{\theta}^{(q)}$ in the $q$th iteration, we have $\boldsymbol{\theta}^H\hat{\mathbf{h}}_m\hat{\mathbf{h}}_m^H\boldsymbol{\theta}\geq 2\Re\left\{\left(\boldsymbol{\theta}^H\right)^{(q)}\hat{\mathbf{h}}_m\hat{\mathbf{h}}_m^H\boldsymbol{\theta}\right\}-\left(\boldsymbol{\theta}^H\right)^{(q)}\hat{\mathbf{h}}_m\hat{\mathbf{h}}_m^H\boldsymbol{\theta}^{(q)}$, which thus follows that

$$\begin{aligned}v_m^{lb}=&2\Re\left\{\left(\boldsymbol{\theta}^H\right)^{(q)}\hat{\mathbf{h}}_m\hat{\mathbf{h}}_m^H\boldsymbol{\theta}+\boldsymbol{\theta}^H\hat{\mathbf{h}}_m\hat{\mathbf{h}}_{m,b}\right\}\rho_m^2\\ &-\left(\boldsymbol{\theta}^H\right)^{(q)}\hat{\mathbf{h}}_m\hat{\mathbf{h}}_m^H\boldsymbol{\theta}^{(q)}\rho_m^2-\sigma^2\gamma^{\mathrm{th}}/P_m.\end{aligned}\tag{20}$$

Furthermore, the unit-modulus constraint (8c) is equivalent to $\left|\theta_n\right|^2\leq 1$ and $\left|\theta_n\right|^2\geq 1$. The non-convex parts of the resulting

constraints are then linearized by

$$\left|\theta_n^{(q)}\right|^2 - 2\Re\left\{(\theta_n^*)^{(q)}\theta_n\right\} \leq -1. \tag{21}$$

Finally, the yielding convex subproblem of the RIS reflection phase shifts $\boldsymbol{\theta}$ is given by

$$\begin{aligned}
\max_{\{\boldsymbol{\theta},\tilde{\mathbf{x}},\tilde{\mathbf{y}},\mathbf{b}\}} \; & P_m\left[2\Re\left\{\left(\boldsymbol{\theta}^H\right)^{(q)}\hat{\mathbf{A}}_m\hat{\mathbf{A}}_m^H\boldsymbol{\theta}\right\}\right. \\
& \left.-\left(\boldsymbol{\theta}^H\right)^{(q)}\hat{\mathbf{A}}_m\hat{\mathbf{A}}_m^H\boldsymbol{\theta}^{(q)}\right] - \lambda^{(q)}\sum_{n=1}^{N+1} b_n \quad (22a) \\
s.t. \quad & \tilde{y}_m\mathbf{I}_K + \left[\left(\eta_m^c\sqrt{1-\rho_m^2}\right)^2 N\right. \\
& \left.+\left(\eta_m^d\sqrt{1-\rho_{m,b}^2}\right)^2\right]\mathbf{I}_K \succeq \mathbf{0}, \forall m, \quad (22b) \\
& \left|\theta_n\right|^2 \leq 1, \forall n, \quad (22c) \\
& \left|\theta_n^{(q)}\right|^2 - 2\Re\left\{(\theta_n^*)^{(q)}\theta_n\right\} \leq b_{n+1} - 1, \forall n, \quad (22d) \\
& \left(\eta_m^c\sqrt{1-\rho_m^2}\right)^2 NK + \left(\eta_m^d\sqrt{1-\rho_{m,b}^2}\right)^2 K \\
& -\sqrt{2\ln(1/p_0)}\tilde{x}_m + \ln(p_0)\,\tilde{y}_m + v_m^{lb} \geq -b_1, \forall m, \quad (22e)
\end{aligned}$$

where $\mathbf{b} = [b_1, ..., b_N, b_{N+1}]^T$ are the introduced slack variables imposed over the associated constraints of the RIS reflection phase shifts $\boldsymbol{\theta}$. $\|\mathbf{b}\|_1$ is the penalty term of the objective function, and is scaled by the penalty factor $\lambda^{(q)}$ to control the feasibility of the constraints. Problem (22) is a convex problem that can be solved by the off-the-shelf tool, such as CVX [31] and MOSEK [33]. The steps of finding a feasible $\boldsymbol{\theta}$ to problem (19) are summarized in Algorithm 1.

***Remark 1:*** Compared with the conventional semi-definite relaxation (SDR) method to design the RIS reflection phase shifts, the motivation of leveraging penalty CCP is that such an approach is able to effectively cope with the constraints associated with $\boldsymbol{\theta}$ that tend to induce the infeasibility of optimization problem. Introducing slack variables can appropriately expand the feasible region of the original problem. Accordingly, the penalty for slack variables in the objective function can effectively enforce such an "expansion". Furthermore, the constraint (8c) in problem (19) can be ensured by the convergence condition $\|\mathbf{b}\|_1 \leq \varepsilon''$ when $\varepsilon''$ is sufficiently small. In addition, the maximum value $\lambda_{\max}$ is imposed to avoid a numerical problem. To be specific, a feasible solution satisfying $\|\mathbf{b}\|_1 \leq \varepsilon''$ may not be found as $\lambda^{(q)}$ increases until the iteration converges to the stopping criteria $\left\|\boldsymbol{\theta}^{(q)} - \boldsymbol{\theta}^{(q-1)}\right\|_1 \leq \varepsilon'$. Thus the convergence of Algorithm 1 can be controlled by the stopping criteria $\left\|\boldsymbol{\theta}^{(q)} - \boldsymbol{\theta}^{(q-1)}\right\|_1 \leq \varepsilon'$.

Finally, based on the AO framework, problem (17) can be solved by solving two approximated subproblems (18) and (22) in an iterative manner. Note that the given point $\boldsymbol{\theta}^{(q)}$ in constraint (22) is updated iteratively in Algorithm 1, which is the same as the penalty factor $\lambda^{(q)}$. While the fixed point $\boldsymbol{\theta}^{(r)}$ in problem (18) is updated iteratively in the outer AO framework. The proposed AO algorithm is elaborated in Algorithm 2.

**Algorithm 1** Penalty CCP-based Optimization for RIS Reflection Phase Shifts

1: **Initialize**: Initialize $\boldsymbol{\theta}^{(0)}$, $\varpi > 1$, and set $q = 0$.
2: **repeat**
3:  **if** $q < Q_{\max}$ **then**
4:  Solving problem (22) and denote the optimal solution as $\boldsymbol{\theta}^{(q+1)}$.
5:  Update $\lambda^{(q+1)} = \min\left\{\varpi\lambda^{(q)}, \lambda_{\max}\right\}$.
6:  $q = q + 1$.
7:  **else**
8:  Reinitialize with a new $\boldsymbol{\theta}^{(0)}$, and set up $\varpi > 1$ and $q = 0$ again.
9:  **end if**
10: **until** $\left\|\boldsymbol{\theta}^{(q)} - \boldsymbol{\theta}^{(q-1)}\right\|_1 \leq \epsilon'$ and $\|\mathbf{b}\|_1 \leq \epsilon''$.
11: **Output**: $\boldsymbol{\theta}^{(r+1)} = \boldsymbol{\theta}^{(q)}$.

### *D. Discussion*

AO is actually a multi-stage iterative optimization algorithm. The outer loop involves two subproblems for optimizing $\mathbf{P}$ and $\boldsymbol{\theta}$, and each subproblem still needs to be solved in an iterative update method. In particular, the complexity of solving the RIS reflection phase shifts based on the penalty CCP method mainly derives from Step 4 of Algorithm 1. In Step 4, solving problem (22) results in a complexity of $\mathfrak{o}_{\boldsymbol{\theta}} = \mathcal{O}\left((MK+2N)^{1/2}n_1\left({n_1}^2 + n_1MK^2 + K^3 + n_1N\right)\right)$ by utilizing the interior point method [34, Lecture 6] [29], where $n_1 = 2N + M + 1$ denotes the number of variables in problem (22). Let $q_{\max}$ be the maximum number that allows Algorithm 1 to converge, and the computational complexity of Algorithm 1 is $q_{\max}\mathfrak{o}_{\boldsymbol{\theta}}$. Similarly, the complexity of Step 3 in Algorithm 2 is $\mathfrak{o}_{\mathbf{P}} = \mathcal{O}\left((MK+2M)^{1/2}n_2\left({n_2}^2 + n_2MK^2 + K^3 + n_2MK^2(K+1)^2\right)\right)$, where $n_2 = M$. Hence, the overall computational complexity of Algorithm 2 is thus equal to $r_{\max}\left(q_{\max}\mathfrak{o}_{\boldsymbol{\theta}} + \mathfrak{o}_{\mathbf{P}}\right)$, where $r_{\max}$ denotes the maximum number of iterations.

Next, the convergence of Algorithm 2 is analyzed as follows. In particular, denoting the objective value of problem (17) as $\Phi(\mathbf{P}, \boldsymbol{\theta}) = P_m\left\|\hat{\mathbf{A}}_m^H\boldsymbol{\theta}\right\|^2$, it follows that

$$\Phi\left(\mathbf{P}^{(r)}, \boldsymbol{\theta}^{(r)}\right) \overset{(a)}{\leq} \Phi\left(\mathbf{P}^{(r+1)}, \boldsymbol{\theta}^{(r)}\right) \overset{(b)}{\leq} \Phi\left(\mathbf{P}^{(r+1)}, \boldsymbol{\theta}^{(r+1)}\right), \tag{23}$$

where (a) comes from the fact that with the given $\boldsymbol{\theta}^{(r)}$, problem (18) is solved optimally with solution $\mathbf{P}^{(r+1)}$. Since there is always a feasible solution $\boldsymbol{\theta}^{(r+1)}$ for problem (22) to maximize the objective function, (b) holds true. Hence, the sequence $\left\{\Phi\left(\mathbf{P}^{(r)}, \boldsymbol{\theta}^{(r)}\right)\right\}$ is non-decreasing and the algorithm is guaranteed to converge.

The idea of alternatingly updating variables is quite straightforward. Such method is widely applicable and in general has good performance, as verified in [8], [16]–[18]. Nonetheless, this approach also has three following drawbacks: i) AO relies on deterministic objective function and constraints. When the studied problem has the nature of stochasticity, i.e., the expectation objective function and probabilistic constraints, the

**Algorithm 2** Proposed AO Algorithm for Solving Problem (17)

1: **Initialize**: $\mathbf{P}^{(0)}$ and $\boldsymbol{\theta}^{(0)}$, and set the iteration index $r=0$.
2: **repeat**
3: Solve problem (18) for given $\boldsymbol{\theta}^{(r)}$, and denote the optimal solution as $\mathbf{P}^{(r+1)}$.
4: Obtain the optimal solution $\boldsymbol{\theta}^{(r+1)}$ via Algorithm 1 for given $\left\{\mathbf{P}^{(r+1)}, \boldsymbol{\theta}^{(r)}\right\}$.
5: $r=r+1$.
6: **until** The change of the objective value is below a threshold $\epsilon'''>0$ or $r \geq r_{\max}$.
7: **Output**: the optimal solution $\left\{\mathbf{P}^{(*)}, \boldsymbol{\theta}^{(*)}\right\}$.

corresponding closed-form expressions must be obtained for a further analysis, which is a major challenge for the multi-VUE situation in which the closed-form expressions are not allowed to be expressed explicitly. ii) The complexity of AO depends on each subproblem's complexity. The overall complexity becomes unacceptable when all the subproblems also require iterative methods. In addition, the accuracy of solution obtained by AO depends on the convergence condition, i.e., a precise enough convergence criterion should be selected in order to prevent from stopping at an uninteresting point. iii) In the single-VUE case, the original stochastic optimization problem is transformed into a deterministic problem according to the statistical characteristics of CSI error. However, it is not appropriate to straightly extend AO to the multi-VUE case under imperfect S-CSI. As a result, a new algorithm with lower complexity, greater robustness, and better extendibility is more than essential for the multi-VUE case.

## IV. Multi-VUE Case

### A. CSSCA for Solving Problem (8)

In this section, we address the multi-VUE case where there in general exists multi-user interference. The interference terms give rise to difficulties of analyzing the closed-form of the average achievable capacity, predominantly due to the fact that the optimal MUD matrix as explicit functions of the RIS phase shifts are prohibitive to obtain. This hinders the beamforming design. A classical approach to deal with the expectation operation of the objective function is the sample average approximation method. Accordingly, we adopt a low-complexity CSSCA optimization framework [14] [35]. The pivotal idea of CSSCA is to construct strongly convex/concave functions for the stochastic objective function and constraints in conformity with the randomly generated channel samples that are based on the S-CSI. The variables are updated by solving a convex problem obtained by replacing the objective and the constraint functions with their convex surrogate functions, based on the statistics of the channels, or a data set containing a large number of channel samples that capture the properties of the considered system. The corresponding steps are elaborated as follows.

*1) Step 1:* For each block in the considered transmission frame, $T_H$ new channel samples $\left\{\mathbf{H}\left[t\right]_{(j)}^{(i)}\right\}_{j=\{1,\ldots,T_H\}} = \left\{\mathbf{h}_m[t]_{(j)}, \mathbf{h}_{m,b}[t]_{(j)}\right\}_{j=\{1,\ldots,T_H\}}^{(i)}$ are randomly generated in the $i$th iteration, where $\mathbf{h}_m[t]_{(j)}$ and $\mathbf{h}_{m,b}[t]_{(j)}$ are defined in (6) and (7). To tackle the outage probability constraint in (8b), we convert it into the following constraint with expectation. By utilizing the step function $u\left(x\right)$, we have

$$\Pr\left(\mathrm{SINR}_m\left[t\right] \leq \gamma^{\mathrm{th}}\right) = \mathbb{E}\left[u\left(\gamma^{\mathrm{th}} - \mathrm{SINR}_m\left[t\right]\right)\right]. \tag{24}$$

Let $\hat{u}_\beta\left(x\right) = \left(1+e^{-\beta x}\right)^{-1}$ be a smooth approximation of the step function with a non-negative smooth parameter $\beta$ that can be used to control the approximation error. For convenience, the set of optimization variables is defined as $\boldsymbol{\mathcal{V}} \triangleq \{\mathbf{P}, \boldsymbol{\theta}, \mathbf{F}\}$. The objective function and the constraint in (8b) can be expressed by $g_{m,0}\left(\boldsymbol{\mathcal{V}}\right) \triangleq \mathbb{E}\left[R_m\left(\boldsymbol{\mathcal{V}}; \mathbf{H}\left[t\right]\right)\right], \forall m,t$, and $g_{m,1}\left(\boldsymbol{\mathcal{V}}\right) \triangleq \mathbb{E}\left[S_m\left(\boldsymbol{\mathcal{V}}; \mathbf{H}\left[t\right]\right)\right] \leq 0, \forall m,t$, respectively, where $S_m\left(\boldsymbol{\mathcal{V}}; \mathbf{H}\left[t\right]\right)$ is shown in (25) at the top of the next page and $R_m\left(\boldsymbol{\mathcal{V}}; \mathbf{H}\left[t\right]\right) = \log_2\left(1+\mathrm{SINR}_m\left[t\right]\right)$. Then, by obtaining new channel samples $\left\{\mathbf{H}\left[t\right]_{(j)}^{(i)}\right\}_{j=\{1,\ldots,T_H\}}$ and the results in the $(i-1)$th iteration $\boldsymbol{\mathcal{V}}^{(i-1)}$, the surrogate functions can be constructed to approximate the non-convex stochastic functions $g_{m,0}\left(\boldsymbol{\mathcal{V}}\right)$ and $g_{m,1}\left(\boldsymbol{\mathcal{V}}\right)$, i.e.,

$$\begin{aligned}\bar{g}_{m,s}^{(i)}\left(\boldsymbol{\mathcal{V}}\right) = {} & \hat{g}_{m,s}^{(i)} + \left(\bar{\mathbf{g}}_{\mathbf{P}}^{(i)}\right)_{m,s}^{T}\left(\mathbf{P}-\mathbf{P}^{(i-1)}\right) \\ & + \Re\left\{\left(\bar{\mathbf{g}}_{\boldsymbol{\theta}}^{(i)}\right)_{m,s}^{H}\left(\boldsymbol{\theta}-\boldsymbol{\theta}^{i-1}\right)\right\} + \mathrm{Tr}\left(\left(\bar{\mathbf{g}}_{\mathbf{F}}^{(i)}\right)_{m,s}^{H}\left(\mathbf{F}-\mathbf{F}^{(i-1)}\right)\right) \\ & - \tau_s\left\|\mathbf{P}-\mathbf{P}^{(i-1)}\right\|^2 - \tau_s\left\|\boldsymbol{\theta}-\boldsymbol{\theta}^{(i-1)}\right\|^2 \\ & - \tau_s \mathrm{Tr}\left(\left(\mathbf{F}-\mathbf{F}^{(i-1)}\right)\left(\mathbf{F}-\mathbf{F}^{(i-1)}\right)^H\right), s=0,1,\end{aligned} \tag{26}$$

where

$$\begin{aligned}\left(\bar{\mathbf{g}}_{\boldsymbol{\mathcal{V}}}^{(i)}\right)_{m,0} = {} & \left(1-\varrho^{(i)}\right)\left(\bar{\mathbf{g}}_{\boldsymbol{\mathcal{V}}}^{(i-1)}\right)_{m,0} \\ & + \varrho^{(i)}\nabla_{\boldsymbol{\mathcal{V}}} R_m\left(\boldsymbol{\mathcal{V}}^{(i-1)}; \mathbf{H}[t]^{(i)}\right),\end{aligned} \tag{27a}$$

$$\begin{aligned}\left(\bar{\mathbf{g}}_{\boldsymbol{\mathcal{V}}}^{(i)}\right)_{m,1} = {} & \left(1-\varrho^{(t)}\right)\left(\bar{\mathbf{g}}_{\boldsymbol{\mathcal{V}}}^{(i-1)}\right)_{m,1} \\ & + \varrho^{(i)}\nabla_{\boldsymbol{\mathcal{V}}} S_m\left(\boldsymbol{\mathcal{V}}^{(i-1)}; \mathbf{H}[t]^{(i)}\right).\end{aligned} \tag{27b}$$

Detailed expressions of $\nabla_{\boldsymbol{\mathcal{V}}} R_m\left(\boldsymbol{\mathcal{V}}^{(i-1)}; \mathbf{H}[t]^{(i)}\right)$ and $\nabla_{\boldsymbol{\mathcal{V}}} S_m\left(\boldsymbol{\mathcal{V}}^{(i-1)}; \mathbf{H}[t]^{(i)}\right)$ in (27a) and (27b) are omitted here due to the limitation of paper length, and they can be easily derived in light of the facts in [36, Sec. 2.4]. The constant $\tau_0 > 0$ is able to guarantee that $\bar{g}_{m,0}^{(i)}\left(\boldsymbol{\mathcal{V}}\right)$ is strongly concave with respect to all variables, and $\tau_1 < 0$ is able to ensure the strong convexity of $\bar{g}_{m,1}^{(i)}\left(\boldsymbol{\mathcal{V}}\right)$ with respect to all variables. $\varrho^{(i)}$ satisfies Assumption 1 (i.e., Assumption 5 in [35]), which will be specified later. For the constant surrogate function, we have

$$\hat{g}_{m,0}^{(i)} = \frac{1}{i}\sum_{j=1}^{i} R_m\left(\boldsymbol{\mathcal{V}}^{(i-1)}; \mathbf{H}\left[t\right]_{(j)}^{(i)}\right), \tag{28a}$$

$$\hat{g}_{m,1}^{(i)} = \frac{1}{i}\sum_{j=1}^{i} S_m\left(\boldsymbol{\mathcal{V}}^{(i-1)}; \mathbf{H}\left[t\right]_{(j)}^{(i)}\right). \tag{28b}$$

$$S_m\left(\boldsymbol{\mathcal{V}};\mathbf{H}\left[t\right]\right)=\hat{u}_\beta\left\{\gamma^{\text{th}}\left(\sum_{m'\in\mathcal{M}\backslash m}P_{m'}\left|\mathbf{f}_m^H\left(\mathbf{h}_{m'}^H\left[t\right]\boldsymbol{\theta}+\mathbf{h}_{m',b}\left[t\right]\right)\right|^2+\sigma^2\left|\mathbf{f}_m^H\right|^2\right)-P_m\left|\mathbf{f}_m^H\left(\mathbf{h}_m^H\left[t\right]\boldsymbol{\theta}+\mathbf{h}_{m,b}\left[t\right]\right)\right|^2\right\}-p_0. \tag{25}$$

Therefore, based on the randomly generated channel samples $\left\{\mathbf{H}\left[t\right]_{(j)}^{(i)}\right\}_{j=\{1,\ldots,T_H\}}$ at the beginning of each iteration and the corresponding solutions obtained in the last iteration $\boldsymbol{\mathcal{V}}^{(i-1)}\triangleq\left\{\mathbf{P}^{(i-1)},\boldsymbol{\theta}^{(i-1)},\mathbf{F}^{(i-1)}\right\}$, the achievable average rate $g_{m,0}\left(\boldsymbol{\mathcal{V}}\right)$, although not expressed explicitly, can be approximated by updating $\left(\bar{\mathbf{g}}_{\boldsymbol{\mathcal{V}}}^{(i)}\right)_{m,s}$ and $\hat{g}_{m,s}^{(i)}\left(s=0,1\right)$ in an iterative manner in (27) and (28). Similar to the single-VUE case, the unit-modulus constraint can be equivalent to $1\leq\left|\theta_n\right|^2\leq1,\forall n$, and the non-convex part can be tackled by linearization as expressed in (21).

*2) Step 2:* In this step, the yielding problem to attain the optimal solution $\{\boldsymbol{\mathcal{V}}\}$ is given by

$$\max_{\{\mathbf{P},\boldsymbol{\theta},\mathbf{F}\}}\quad\sum_{m\in\mathcal{M}}\bar{g}_{m,0}^{(i)}\left(\boldsymbol{\mathcal{V}}\right) \tag{29a}$$

$$s.t.\quad 0\leq P_m\leq P_{\max},\forall m, \tag{29b}$$

$$\bar{g}_{m,1}^{(i)}\left(\boldsymbol{\mathcal{V}}\right)\leq0,\forall m, \tag{29c}$$

$$\left|\theta_n\right|^2\leq1,\forall n, \tag{29d}$$

$$\left|\theta_n^{(i)}\right|^2-2\Re\left\{\left(\theta_n^*\right)^{(i)}\theta_n\right\}\leq-1,\forall n. \tag{29e}$$

Problem (29) is allowed to be viewed as a convex approximation of problem (8). However, problem (29) does not always have a feasible solution. If it turns out to be infeasible, the following surrogate problem is indispensable and solved as the current update

$$\min_{\{\mathbf{P},\boldsymbol{\theta},\mathbf{F},\iota\}}\quad\iota \tag{30a}$$

$$s.t.\quad\bar{g}_{m,1}^{(i)}\left(\boldsymbol{\mathcal{V}}\right)\leq\iota,\forall m, \tag{30b}$$

$$\left|\theta_n\right|^2-1\leq\iota,\forall n, \tag{30c}$$

$$\left|\theta_n^{(i)}\right|^2-2\Re\left\{\left(\theta_n^*\right)^{(i)}\theta_n\right\}+1\leq\iota,\forall n. \tag{30d}$$

Let $\bar{\boldsymbol{\mathcal{V}}}\triangleq\left\{\bar{\mathbf{P}},\bar{\boldsymbol{\theta}},\bar{\mathbf{F}}\right\}$ be the set of solutions for problem (30) when (29) is infeasible. Note that optimizing $\mathbf{P}$, $\boldsymbol{\theta}$ and $\mathbf{F}$ in problem (29) is able to maximize the achievable average rate since $\bar{g}_0^{(i)}\left(\boldsymbol{\mathcal{V}}\right)$ is a function of the optimization variable. While by solving problem (30), we approximately minimize the gap between $\Pr\left(\text{SINR}_m\left(\boldsymbol{\mathcal{V}};\mathbf{H}[t]\right)\leq\gamma^{\text{th}}\right)$ and the corresponding outage probability $p_0$, i.e., $\iota$, which helps to push the solution to the feasible region when the current problem is infeasible in the $i$th iteration. It can be seen that both problems (29) and (30) are convex, which can be efficiently solved by off-the-shelf solvers, such as MOSEK [33].

*3) Step 3:* After obtaining $\bar{\boldsymbol{\mathcal{V}}}$, $\boldsymbol{\mathcal{V}}$ can be updated according to

$$\boldsymbol{\mathcal{V}}^{(i)}=\left(1-\zeta^{(i)}\right)\boldsymbol{\mathcal{V}}^{(i-1)}+\zeta^{(i)}\bar{\boldsymbol{\mathcal{V}}}^{(i)}, \tag{31}$$

where $\zeta^{(i)}$ is an iteration-dependent constant that satisfies the following assumption [35, Assumption 5] (referred to Assumption 1): i) $\varrho^{(i)}\to0,\sum_i\left(\varrho^{(i)}\right)^2<\infty$; ii) $\zeta^{(i)}\to0$, $\sum_i\zeta^{(i)}=0$, $\sum_i\left(\zeta^{(i)}\right)^2\leq\infty$; and iii) $\lim_{i\to\infty}\frac{\zeta^{(i)}}{\varrho^{(i)}}=0$. The above process repeats iteratively until convergence, which yields the proposed JAPMC algorithm as summarized in Algorithm 3.

**Algorithm 3** **J**oint optimization of **A**ctive and **P**assive beamforming in the **M**ulti-VUE case by leveraging **C**SSCA (JAPMC)

1: **Input**: $\left\{\varrho^{(i)}\right\}$, $\left\{\zeta^{(i)}\right\}$ and $T_H$. **Initialize**: $\boldsymbol{\mathcal{V}}^{(0)}$ and $i=1$.
2: **repeat**
3: Generate $T_H$ new channel samples according to the true CSI $\mathbf{H}[t]$ at the $t$th block.
4: Update surrogate functions according to (26).
5: Obtain the optimal $\boldsymbol{\mathcal{V}}^{(i)}$ by solving problem (29) if (29) is feasible. Otherwise solve problem (30) to obtain $\bar{\boldsymbol{\mathcal{V}}}$.
6: Update $\boldsymbol{\mathcal{V}}^{(i)}$ according to (31).
7: $i=i+1$.
8: **until** The convergence criteria is met.
9: **Output**: the optimal solution $\boldsymbol{\mathcal{V}}\triangleq\{\mathbf{P},\boldsymbol{\theta},\mathbf{F}\}$.

The proposed JAPMC algorithm tends to yield a faster convergence speed, not only due to the fact that it provides much freedom to design good surrogate functions for the case of interest, but also because it iteratively optimizes a sequence of surrogate functions with strong convexity/concavity [35]. It is important to mention that JAPMC only requires the per-block S-CSI to solve problem (8), i.e., resorting to the per-block S-CSI to generate the channel samples $\left\{\mathbf{H}\left[t\right]_{(j)}^{(i)}\right\}_{j=\{1,\ldots,T_H\}}$ for the stochastic optimization, which is practically engaging due to the undesirable channel estimation overhead in the RIS-aided high mobility system, especially for a large $N$ and the easily outdated CSI.

### *B. Convergence and Complexity of JAPMC*

This subsection mainly discusses the convergence and computational complexity of the proposed JAPMC. First of all, the convergence of JAPMC is analyzed as follows. It is supposed that $\boldsymbol{\mathcal{V}}^{(0)}\triangleq\left\{\mathbf{P}^{(0)},\boldsymbol{\theta}^{(0)},\mathbf{F}^{(0)}\right\}$ are the feasible initial points for problem (8), i.e., satisfying the probabilistic constraint $\Pr\left(\text{SINR}_m\left(\boldsymbol{\mathcal{V}}^{(i-1)};\mathbf{H}[t]^{(i)}\right)\leq\gamma^{\text{th}}\right)\leq p_0,\forall m,t$. Let $\left\{\boldsymbol{\mathcal{V}}^{(i)}\right\}_{i=1}^{\infty}$ denote the values iteratively generated by JAPMC with a sufficiently small initial step size $\zeta^{(0)}$, then each limit point $\boldsymbol{\mathcal{V}}^{(*)}$ of $\left\{\boldsymbol{\mathcal{V}}^{(i)}\right\}_{i=1}^{\infty}$ is a stationary point of problem (8). In addition, JAPMC is able to almost surely convergence to the set of stationary solutions of problem (8), and a detailed proof can be found in [15] [35] .

Next, let us analyze the computational complexity of JAPMC, the complexity of which primarily stems from the update of $\boldsymbol{\mathcal{V}}^{(i)}$ and $\bar{\boldsymbol{\mathcal{V}}}^{(i)}$ in Step 5. Besides, both problems (29) and (30) can be expressed as a second-order cone program (SOCP), and the complexity of solving them by utilizing a standard interior-point method [29] can be shown as $\mathfrak{o} = \mathcal{O}\left(\sqrt{2\left(M+N\right)}n\left(n^2+n\left(M\left(M+N+K^2\right)+N\right)\right)\right)$, where $n = M+N$ is the number of variables. Accordingly, the complexity for jointly updating the transmit power $\mathbf{P}$, the RIS phase shifts $\boldsymbol{\theta}$ and the MUD matrix $\mathbf{F}$ is $t_{\max}\mathfrak{o}$, where $t_{\max}$ denotes the maximum iteration number required by JAPMC.

## V. Simulation Results

In this section, simulation results are presented to validate the proposed transmission schemes for the RIS-aided mmWave vehicular communication system and some useful insights are drawn. We customize our simulation following the evaluation methodology for the freeway case defined in 3GPP TR 36.885 [37, Annex A], which describes in detail vehicle drop models, densities, speeds, and directions of movement. The considered system operates at 28 GHz with bandwidth $B = 500$ MHz. The mmWave channel parameters of distance-dependent path loss is set to $\mathrm{PL}_0 = 61.4$ dB and $\sigma_s^2 = 5.8$ dB [38] [39]. We configure $\alpha_{m,b} = 3$, $\alpha_{m,r} = 2.2$ and $\alpha_{r,b} = 2.5$ [8], i.e., the path-loss exponent of the BS-VUE link is larger than that of the BS-RIS and RIS-VUE link, to model the scenario that the VUEs suffer from severe signal attenuation in the BS-VUE direct link. The three-dimensional coordinates of the BS and the RIS in meters are $(0,0,25)$ and $(50,0,25)$, respectively. The BS is equipped with $K = 16$ antennas, and the total number of RIS reflecting elements is $N{=}N_{\mathrm{h}}\times N_{\mathrm{v}}$ $(30 = 5\times 6)$, in which the active and the passive antenna spacing of both are $d = \lambda_c/2$ ($\lambda_c$ denotes the wavelength). For the statistical CSI error model, the variances of $\mathrm{vec}\left(\Delta\mathbf{h}_m\right)$ and $\Delta\mathbf{h}_{m,b}$ are defined as $\left(\eta_m^c\right)^2 = \left(\delta^c\right)^2\left\|\mathrm{vec}\left(\hat{\mathbf{h}}_m\right)\right\|_2^2$ and $\left(\eta_m^d\right)^2 = \left(\delta^d\right)^2\left\|\hat{\mathbf{h}}_{m,b}\right\|_2^2$, respectively. $\delta^c \in [0,1)$ and $\delta^d \in [0,1)$ measure the relative amount of CSI uncertainties. Other system parameters are set as follows unless specified otherwise: $\sigma^2 = -80$ dBm, $L_{m,b} = L_{r,b} = L_{m,r} = 3$, $P_{\max} = 23$ dBm, $v = 140$ km/h, $p_0 = 0.001$, $\gamma^{\mathrm{th}} = 12$ dB, $\delta^c = 0.01$, and $\delta^d = 0.02$. The temporal correlation coefficient is $\rho\left(T_s\right) = 0.986$ (when $v = 140$ km/h and $T_s = 10$ us) and the Doppler shifts $\{f_{m,b,l}, f_{m,r,l}\}$ are uniformly distributed in $[0, f_{\max}]$ [21]. For the single-VUE case, we let $M = 1$, i.e., select one VUE randomly from the generated vehicles. For the multi-VUE case, the corresponding parameters are: $M = 5$, $T_H = 300$, $\rho^{(0)} = 0, \rho^{(i)} = \frac{1}{(1+i)^{2/3}}$, $\beta = 10^5$, $\zeta^{(i)} = \frac{2}{2+i}$, and $|\tau_s| = 0.5$.

### A. Single-VUE Case

Figure 3 shows the convergence behavior of Algorithm 2 with different number of RIS reflecting elements. The convergence condition is $\left(\Phi^{(r+1)} - \Phi^{(r)}\right)/\Phi^{(r)} \le \varepsilon'''$ $\left(\varepsilon''' = 10^{-8}\right)$. It can be observed from Fig. 3 that the proposed AO algorithm is monotonically convergent, which is in good agreement with the theoretical analysis of convergence behavior. At the same time, the proposed algorithm converges rapidly and 6 iterations are sufficient for the algorithm to converge. In addition, a larger $N$ allows the algorithm to converge to a higher value, which benefits from the passive beamforming gain of the RIS.

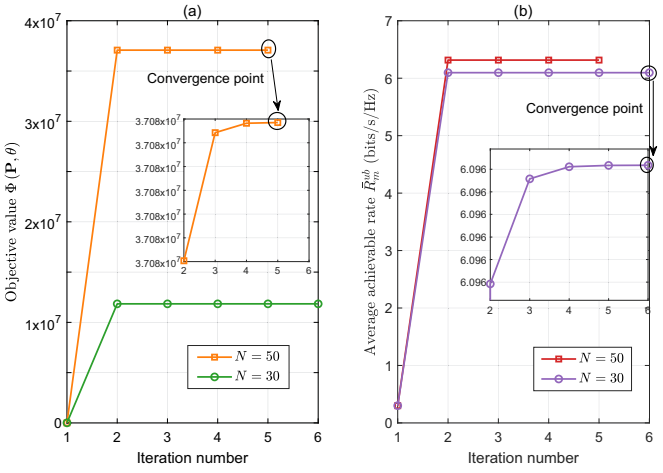


Fig. 3. Convergence behaviors of Algorithm 2 for different number of RIS reflecting elements $N$.

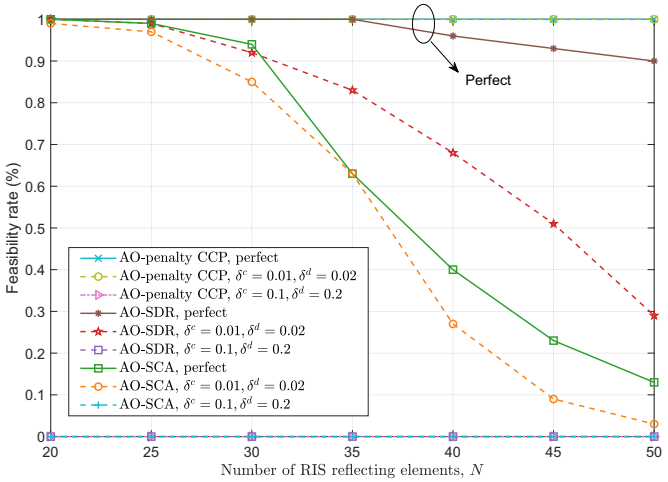


Fig. 4. Feasibility rate versus the number of RIS reflecting elements $N$ for different algorithms and CSI uncertainties.

In order to demonstrate the superiority of the proposed penalty-CCP-based algorithm (Algorithm 1) in terms of searching for feasible solutions with respect to RIS reflection phase shifts, the commonly methods in use, such as conventional SDR [16] [17] and successive convex approximation (SCA) [8], are served as benchmark schemes. We compare in Fig. 4 the feasibility rate of each algorithm under three CSI uncertainties (i.e., perfect CSI, $\delta^c = 0.01$, $\delta^d = 0.02$, and $\delta^c = 0.1$, $\delta^d = 0.2$, respectively). Feasibility rate is defined as the ratio of the number of feasible channel to the total number of channel generations, where a feasible channel implies that there exists a feasible solution for the

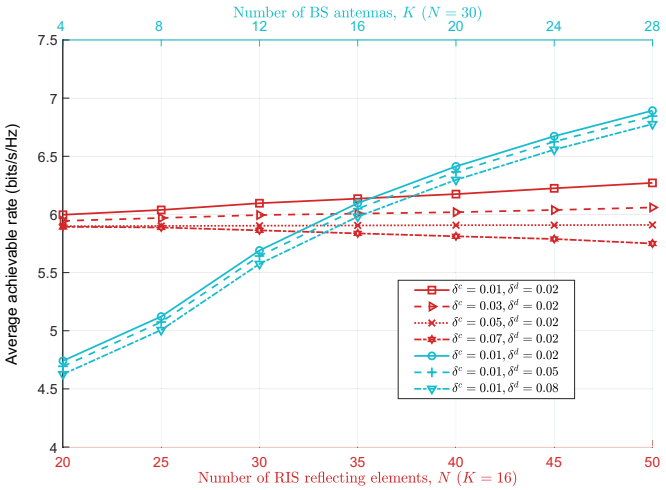


Fig. 5. Average achievable rate versus the number of BS antennas $K$ & reflecting elements $N$ in the single-VUE case.

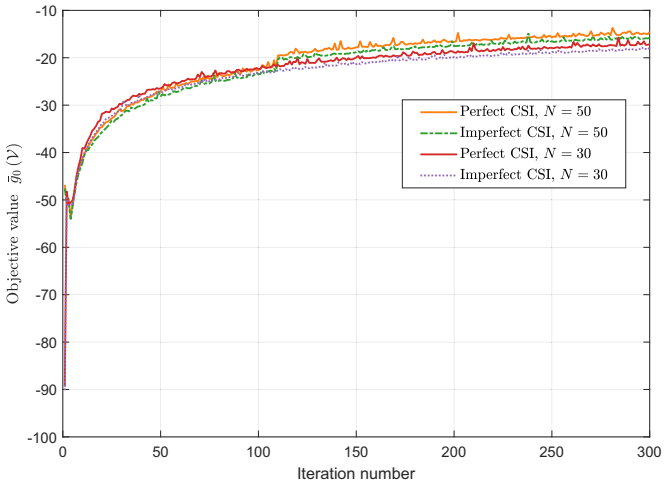


Fig. 6. Convergence behaviors of JAPMC.

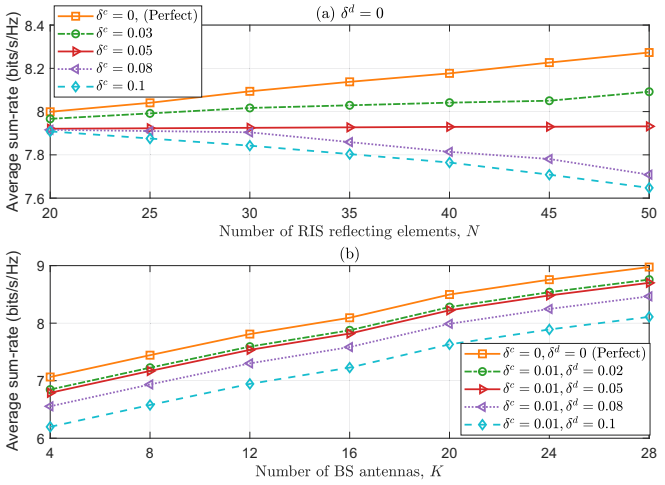


Fig. 7. Average sum-rate versus the number of BS antennas $K$ & reflecting elements $N$ in the multi-VUE case.

optimization problem under this channel generation[1]. An eye-catching phenomenon in Fig. 4 is that there is no feasible solution for three options when the CSI uncertainty level is high, i.e., $\delta^c = 0.1$, $\delta^d = 0.2$. Meanwhile, the better the CSI, the higher the feasibility rate, which implies that the algorithm performance is greatly affected by the CSI uncertainty. In addition, under perfect CSI and a low-level CSI uncertainty (e.g., $\delta^c = 0.01, \delta^d = 0.02$), the proposed AO-penalty CCP, compared to the other two schemes, always shows a fairly high feasibility rate, i.e., almost approaches to 100% as $N$ increases, while both SDR and SCA, the performance of which fluctuate with varying $N$, are largely affected by CSI. This agrees with the discussion in Remark 1, and also demonstrates the robustness and superiority of our proposed algorithm.

Figure 5 plots the average achievable rate versus the number of BS antennas $K$ and the number of RIS reflecting elements $N$ under different CSI uncertainties. First, we investigate the situation that the BS antennas is fixed at $K = 16$. When the CSI uncertainty level is low, e.g., $\delta^c = \{0.01, 0.03, 0.05\}, \delta^d = 0.02$, the average achievable rate increases in varying degrees with an increment of $N$, while it deteriorates under higher CSI uncertainties as $N$ increases. This is a noteworthy finding and the reasons are analyzed as follows. An increasing number of RIS reflecting elements give rise to a considerable gain in terms of the average achievable rate due to the passive beamforming. However, a larger $N$ leads to a higher channel estimation error under a high CSI uncertainty, which hinders the improvement of system performance as $N$ grows. Second, when fixing $N = 30$, the other insight observed from Fig. 5 is that although the increment of CSI uncertainty results in the loss of system rate, the average achievable rate still raises as the number of BS antennas $K$ grows. This is attributed to the fact that the benefits brought by the increase of $K$ outweigh its drawbacks, which can compensate for system performance under different CSI uncertainties.

[1]It should be noted that one iteration with a feasible solution in general has considerable dependence on parameter initialization, channel conditions and algorithm design.

### B. Multi-VUE Case

The convergence behavior of our proposed JAPMC is illustrated in Fig. 6 by depicting that the objective value $\sum_{m \in \mathcal{M}} \bar{g}_{m,0}(\boldsymbol{\mathcal{V}})$ varies with the number of iterations under different settings of CSI and $N$. Due to the stochastic nature of the studied problem and the proposed algorithm, the objective value curves in Fig. 6 are not monotonous and fluctuate in a small range. However, it can be seen from the overall trend that the curves gradually increase and exhibit trend of convergence after about 250 iteration times. Meanwhile, compared with perfect CSI, the schemes under imperfect CSI suffer a certain loss of system performance.

The impact of CSI acquisition accuracy on system performance in the multi-VUE case is illustrated in Fig. 7 that depicts the average sum-rate versus the number of RIS reflecting elements $N$. In order to intuitively explore the impact

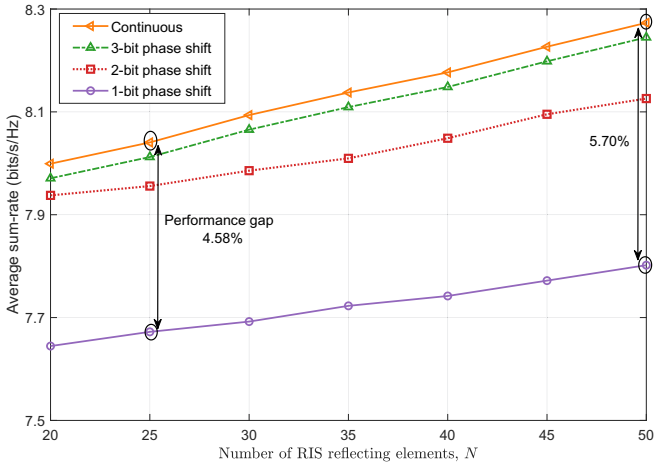


Fig. 8. Average sum-rate versus different number of reflecting elements $N$ under different discrete phase shifts.

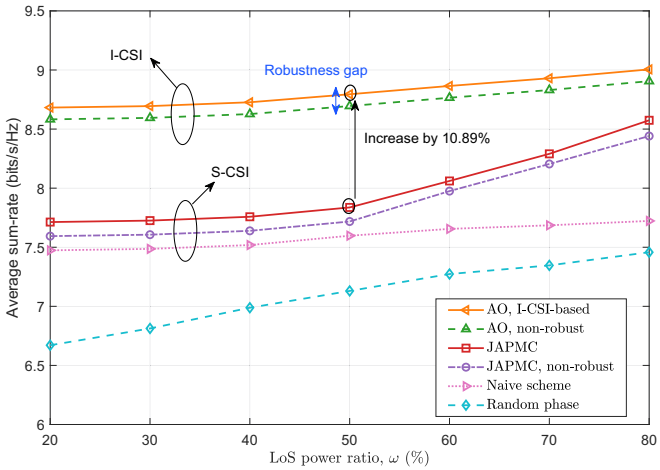


Fig. 9. Average sum-rate versus LoS power ratio $\omega$.

of the variation of $N$ with diverse CSI uncertainties of the cascaded channels on the average sum-rate, specifically, we set $\delta^d = 0$ in Fig. 7(a) (i.e., assuming that the direct channel is perfect). From Fig. 7(a), it can be observed that a high CSI uncertainty has a great influence on the improvement of system performance as $N$ increases. This is because more RIS reflecting elements bring higher CSI error, which degrades the system performance. By contrast, we find in Fig. 7(b) that the increment of the number of antennas $K$ at the BS is effective in boosting the average sum-rate, arriving at the same conclusion as that of the single-VUE case. In conjunction with the observations in the single- and multi-VUE case, we conclude that a large number of reflecting elements at the RIS, presumably resulting in a high average rate, should be taken with a grain of salt: Within a reasonable region of CSI uncertainty change, the gain brought by the passive beamforming is good, which, however, suffers from noticeable degradation if the CSI uncertainty grows beyond the acceptable margin.

It is worth noting that the phase shifts are usually discrete due to hardware limitations in the practical system [40]. Our proposed algorithms provide, therefore, the best-case bound for realistic scenarios and have the potential to be extended to discrete phases. An intuitive solution is to round the continuous phase shift obtained to its nearest discrete phase shift, which, however, imposes a performance loss due to the quantization effect. In this regard, Fig. 8 shows the impact of discrete phase shifts at the RIS on average sum-rate. Particularly, we consider, respectively, 1-bit phase shift $\{0, \pi\}$, 2-bit phase shift $\left\{0, \frac{\pi}{2}, \pi, \frac{3}{2}\pi\right\}$, 3-bit phase shift $\left\{0, \frac{\pi}{4}, \frac{\pi}{2}, \pi, \frac{5}{4}\pi, \frac{3}{2}\pi, \frac{5}{4}\pi, \frac{7}{4}\pi\right\}$ by employing JAPMC. It is observed from Fig. 8 that using RIS with 3-bit phase shifts incurs inconspicuous performance loss. In addition, the performance gap between the continuous phases-shift case and low-resolution phase-shift case becomes larger with an increment of $N$. More accurate phase shifts are essential, which, however, tends to make the hardware implementation more challenging. Thus, the trade-off between the overhead and the resolution should be concerned reasonably.

For the next evaluations, the following several benchmarks are adopted for comparison. i) I-CSI-based scheme: particularly, similar to the single-VUE case, the MUD matrix is designed by MRC[2] and the RIS reflection phase shifts are optimized by penalty-CCP method, both of which are updated in an alternating iterative manner. ii) Non-robust scheme: the estimated CSI, i.e., $\left\{\hat{\mathbf{h}}_{m,b}\left[t-T_s\right], \hat{\mathbf{h}}_m\left[t-T_s\right]\right\}$ is treated as perfect CSI. iii) Naive scheme: the channel samples are only updated in the first iteration of JAPMC. iv) A random phase scheme in which $\boldsymbol{\theta}$ is not optimized in JAPMC. iv) The MUD matrix is designed by MRC under the I-CSI without the aid of the RIS.

In Fig. 9, we investigate the average sum-rate achieved by different schemes versus the LoS power ratio. The LoS power ratio of the BS-VUE link is defined as $\omega_{m,b} = \frac{\left|h_{m,b,1}\mathbf{a}_L\left(\vartheta^{\mathrm{AoA}}_{m,b,1}\right)\right|}{\sum_{l=1}^{L_{m,b}}\left|h_{m,b,l}\mathbf{a}_L\left(\vartheta^{\mathrm{AoA}}_{m,b,l}\right)\right|^2}$ [15], and the LoS power ratios of BS-RIS and RIS-VUE links are defined by the similar procedure and are denoted by $\omega_{m,r}$ and $\omega_{r,b}$, respectively. We set $\omega_{m,r} = \omega_{r,b} = \omega$ and $\omega_{m,b} = 0$. First, it is obvious that the average sum-rate achieved by the I-CSI-based scheme is superior to that of the S-CSI-based scheme, manifesting a joint effect of the better multi-VUE interference suppression capability of the AO scheme, the performance gap among which reduces as the LoS power ratio $\omega$ decreases. The performance gap will not approach zero under the considered simulation settings. This is due to the fact that multi-VUE interference is the critical bottleneck in the multi-VUE case, and that the average sum-rate drastically deteriorates, provided that I-CSI is not considered for the design of the RIS reflection coefficients. Second, there always exist performance gaps between the robust and non-robust scheme under the I-CSI- and the S-CSI-based cases, respectively. This evinces, as expected, that the outdated estimated CSI gives rise to the performance loss. The feedback of outdated CSI leads to the

[2]The weighted minimum mean-squared error (WMMSE) algorithm may be more suitable for the beamforming design in multi-VUE case. In order to reduce complexity, here, we adopt MRC to design MUD matrix at the BS [13].

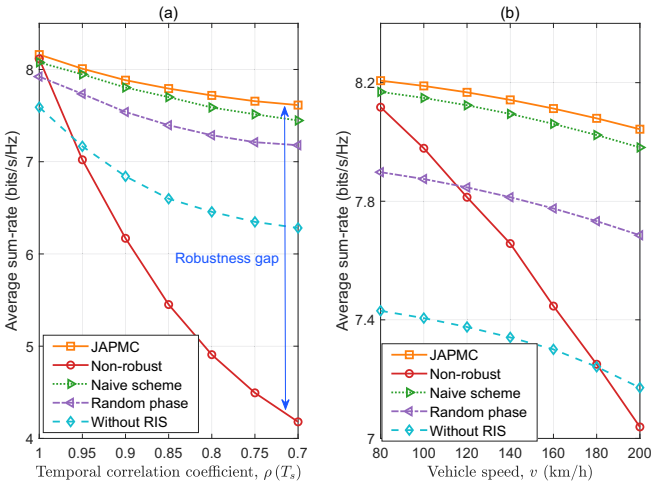


Fig. 10. Impact of temporal correlation coefficient $\rho(T_s)$ and vehicle speed $v$ on average sum-rate.

suboptimal beamforming, thus causing the average sum-rate to fade compared with robust scheme. Third, the average sum-rate obtained by JAPMC gradually enlarges as $\omega$ grows larger. When $\omega$ increases, the performance improvement obtained by JAPMC becomes pronounced mainly because of the reduction in the degree of randomization of multi-VUE interference. Another important reason for the improved performance is that the cascaded link becomes more deterministic as $\omega$ increases, thus rendering the beamforming to be more effective, which underscores the importance of joint active and passive beamforming optimization.

Finally, we analyze how the average sum-rate is affected by the temporal correlation coefficient $\rho(T_s)$ and vehicle speed $v$ in Fig. 10 to substantiate the robustness of our proposed JAPMC. Note that as $\rho(T_s)$ decreases, the CSI becomes more outdated as shown in (6) and (7), and $\rho(T_s) = 1$ means non-outdated CSI. Intuitively, as illustrated in Fig. 10(a), the average sum-rates of all schemes degrade as CSI becomes more outdated, and what is striking is that the non-robust scheme suffers from noticeable degradation and the situation is much worse than that of JAPMC. Besides, the decrease of $\rho(T_s)$ has more effects on the performance of other several schemes while our proposed JAPMC retains the average sum-rate at a favorable level, revealing that benchmark schemes are more sensitive to the uncertainty of CSI and the robustness of JAPMC. Fig. 10(b) plots the average sum-rate versus vehicle speed $v$. Since $\rho(T_s)$ is a function of $v$ and decreases as $v$ increases, the average sum-rate degenerates as $v$ grows larger, which implies that a larger speed presumably endows the acquisition of real-time CSI with more difficulty. That said, we can still validate the advantage of the proposed JAPMC since it outperforms other schemes and the average sum-rate drops slowly compared with a dramatic decline in non-robust scheme. This further verifies that the proposed JAPMC is more robust against mobility-induced CSI uncertainty.

## VI. Conclusion

In this paper, we study the robust transmission for RIS-aided mmWave vehicular communications over time-varying channels. By taking account of the unavailability of full accuracy I-CSI in the high-mobility scenario, a novel transmission protocol is proposed by exploiting the imperfect knowledge of S-CSI. Then, the uplink average achievable rate is maximized, subject to the outage probability and RIS's unit-modulus constraints. Effective robust beamforming algorithms are proposed for the single- and multi-VUE cases, and useful insights are drawn via theoretical analysis. Simulation results substantiate that the system performance is greatly affected by the accuracy of CSI, and the increasing number of RIS elements may hamper the performance improvement when CSI uncertainty is fairly high. In addition, the proposed S-CSI scheme can significantly reduce signal processing complexity and channel training overhead, but there is still a certain performance weakness compared with the I-CSI scheme, which unveils the trade-off between the acquisition scale of CSI and system performance. RIS-aided high mobility scenario is an important topic, and for future work, we will shed light on more effective and efficient communication protocol and transmission design for the RIS-aided high-mobility communications.

## Appendix A
## Proof of Proposition 1

By plugging the optimal MUD matrix $\mathbf{f}_m^{\text{opt}}$ into the objective function of (9), the achievable ergodic rate of the $m$th VUE can be formulated as

$$\begin{aligned}\bar{R}_m &= \mathbb{E}\left\{\log_2\left(1+\frac{P_m}{\sigma^2}\left\|\mathbf{h}_m^H\boldsymbol{\theta}+\mathbf{h}_{m,b}\right\|^2\right)\right\}\\ &\overset{(a)}{\leq} \log_2\left(1+\frac{P_m}{\sigma^2}\mathbb{E}\left\{\left\|\mathbf{h}_m^H\boldsymbol{\theta}+\mathbf{h}_{m,b}\right\|^2\right\}\right),\end{aligned} \tag{32}$$

where (a) comes from Jensen's inequality. Next we focus on the property of $\mathbb{E}\left\{\left\|\mathbf{h}_m^H\boldsymbol{\theta}+\mathbf{h}_{m,b}\right\|^2\right\}$:

$$\begin{aligned}&\mathbb{E}\left\{\left\|\mathbf{h}_m^H\boldsymbol{\theta}+\mathbf{h}_{m,b}\right\|^2\right\}\\ =&\mathbb{E}\left\{\left[\left(\rho_m\hat{\mathbf{h}}_m+\Delta\mathbf{h}_m\right)^H\boldsymbol{\theta}+\rho_{m,b}\hat{\mathbf{h}}_{m,b}+\Delta\mathbf{h}_{m,b}\right]^H\right.\\ &\left.\times\left[\left(\rho_m\hat{\mathbf{h}}_m+\Delta\mathbf{h}_m\right)^H\boldsymbol{\theta}+\rho_{m,b}\hat{\mathbf{h}}_{m,b}+\Delta\mathbf{h}_{m,b}\right]\right\}\\ =&\mathbb{E}\left\{\left[\left(\rho_m\hat{\mathbf{h}}_m^H\boldsymbol{\theta}+\rho_{m,b}\hat{\mathbf{h}}_{m,b}\right)+\left(\Delta\mathbf{h}_m^H\boldsymbol{\theta}+\Delta\mathbf{h}_{m,b}\right)\right]^H\right.\\ &\left.\times\left[\left(\rho_m\hat{\mathbf{h}}_m^H\boldsymbol{\theta}+\rho_{m,b}\hat{\mathbf{h}}_{m,b}\right)+\left(\Delta\mathbf{h}_m^H\boldsymbol{\theta}+\Delta\mathbf{h}_{m,b}\right)\right]\right\}\\ =&\mathbb{E}\left\{\left\|\rho_m\hat{\mathbf{h}}_m^H\boldsymbol{\theta}+\rho_{m,b}\hat{\mathbf{h}}_{m,b}\right\|^2\right\}+\mathbb{E}\left\{\left\|\Delta\mathbf{h}_m^H\boldsymbol{\theta}+\Delta\mathbf{h}_{m,b}\right\|^2\right\}.\end{aligned} \tag{33}$$

For simplicity, it is assumed that $\hat{h}_{r,b,i}$, $\hat{h}_{m,r,j}$ and $\hat{h}_{m,b,l}$ are independent[3] of each other [9] [14]. The first term of (33),

[3]Due to the difficulties of attaining the dependence of associated channels, a *probability-box (p-box)* [41] can be constructed as the envelope of the various distributions composed of the products of random variables by analyzing probability bounds. In accordance with the facts in [42], the independence assumption we made provides a proper subset of the general case, which also contributes meaningful theoretical insights.

i.e., $\mathbb{E}\left\{\left\|\rho_m\hat{\mathbf{h}}_m^H\boldsymbol{\theta}+\rho_{m,b}\hat{\mathbf{h}}_{m,b}\right\|^2\right\}$, can be written as

$$\begin{aligned}
&\mathbb{E}\left\{\left\|\rho_m\hat{\mathbf{h}}_m^H\boldsymbol{\theta}+\rho_{m,b}\hat{\mathbf{h}}_{m,b}\right\|^2\right\}\\
=&\mathbb{E}\left\{\left\|\rho_m\hat{\mathbf{h}}_{r,b}\boldsymbol{\Theta}\hat{\mathbf{h}}_{m,r}+\rho_{m,b}\hat{\mathbf{h}}_{m,b}\right\|^2\right\}\\
=&\varpi_m\mathbb{E}\left\{\left\|\sum_{i=1}^{L_{r,b}}\sum_{j=1}^{L_{m,r}}\hat{h}_{r,b,i}\hat{h}_{m,r,j}\hat{\mathbf{A}}_{r,b,i}\boldsymbol{\Theta}\hat{\mathbf{A}}_{m,r,j}\right\|^2\right\}\\
&+\varpi_{m,b}\mathbb{E}\left\{\left\|\sum_{l=1}^{L_{m,b}}\hat{h}_{m,b,l}\hat{\mathbf{A}}_{m,b,l}\right\|^2\right\},
\end{aligned}\tag{34}$$

where $\mathbf{A}_{r,b,i}=\mathbf{a}_L\left(\vartheta_{r,b,i}^{\mathrm{AoA}}\right)\mathbf{a}_P^H\left(\vartheta_{r,b,i}^{\mathrm{AoD}},\phi_{r,b,i}^{\mathrm{AoD}}\right)\in\mathbb{C}^{K\times N},\forall i$, $\mathbf{A}_{m,r,j}=\mathbf{a}_P\left(\vartheta_{m,r,j}^{\mathrm{AoA}},\phi_{m,r,j}^{\mathrm{AoA}}\right)\in\mathbb{C}^{N\times 1},\forall m,j$, $\mathbf{A}_{m,b,l}=\mathbf{a}_L\left(\vartheta_{m,b,l}^{\mathrm{AoA}}\right)\in\mathbb{C}^{K\times 1},\forall m,l$, $\varpi_m=\frac{\rho_m^2}{L_{r,b}L_{m,r}}\left(\sum_{j=1}^{L_{m,r}}\exp\{j2\pi f_{m,r,j}tT_s\}\right)^2$, $\varpi_{m,b}=\frac{\rho_{m,b}^2}{L_{m,b}}\times\left(\sum_{l=1}^{L_{m,b}}\exp\{j2\pi f_{m,b,l}tT_s\}\right)^2$, and $\hat{\mathbf{A}}$ is the estimation of $\mathbf{A}$. By defining random variables $|h_{r,b}|\triangleq\left|\sum_{i=1}^{L_{r,b}}h_{r,b,i}\right|\sim\mathcal{N}\left(0,\sum_{i=1}^{L_{r,b}}10^{-0.1\mathrm{PL}_{r,b,i}}\right)$, $|h_{m,r}|\triangleq\left|\sum_{j=1}^{L_{m,r}}h_{m,r,j}\right|\sim\mathcal{N}\left(0,\sum_{j=1}^{L_{m,r}}10^{-0.1\mathrm{PL}_{m,r,j}}\right)$, and $|h_{m,b}|\triangleq\left|\sum_{l=1}^{L_{m,b}}h_{m,b,l}\right|\sim\mathcal{N}\left(0,\sum_{l=1}^{L_{m,b}}10^{-0.1\mathrm{PL}_{m,b,l}}\right)$, we have

$$\begin{aligned}
&\mathbb{E}\left\{\left\|\sum_{i=1}^{L_{r,b}}\sum_{j=1}^{L_{m,r}}\hat{h}_{r,b,i}\hat{h}_{m,r,j}\hat{\mathbf{A}}_{r,b,i}\boldsymbol{\Theta}\hat{\mathbf{A}}_{m,r,j}\right\|^2\right\}\\
&=\left\|\sum_{i=1}^{L_{r,b}}\sum_{j=1}^{L_{m,r}}\hat{\mathbf{A}}_{r,b,i}\boldsymbol{\Theta}\hat{\mathbf{A}}_{m,r,j}\right\|^2\mathbb{E}\left\{\left|\hat{h}_{m,r}\right|^2\right\}\cdot\mathbb{E}\left\{\left|\hat{h}_{r,b}\right|^2\right\},
\end{aligned}\tag{35a}$$

$$\mathbb{E}\left\{\left\|\sum_{l=1}^{L_{m,b}}\hat{h}_{m,b,l}\hat{\mathbf{A}}_{m,b,l}\right\|^2\right\}=\left\|\sum_{l=1}^{L_{m,b}}\hat{\mathbf{A}}_{m,b,l}\right\|^2\mathbb{E}\left\{\left|\hat{h}_{m,b}\right|^2\right\}.\tag{35b}$$

Since the square of the modulus of a complex Gaussian random variable with zero mean tends to follow a central chi-square distribution with a degree of freedom (DoF) of 2, i.e., $\left|\hat{h}_{m,b}\right|^2\sim\frac{1}{2}\sum_{l=1}^{L_{m,b}}10^{-0.1\mathrm{PL}_{m,b,l}}\chi^2(2)$ [43], we have $\mathbb{E}\left\{\left|\hat{h}_{m,b}\right|^2\right\}=\sum_{l=1}^{L_{m,b}}10^{-0.1\mathrm{PL}_{m,b,l}}$. Similarly, it follows that $\mathbb{E}\left\{\left|\hat{h}_{m,r}\right|^2\right\}=\sum_{j=1}^{L_{m,r}}10^{-0.1\mathrm{PL}_{m,b,j}}$ and $\mathbb{E}\left\{\left|\hat{h}_{r,b}\right|^2\right\}=\sum_{i=1}^{L_{r,b}}10^{-0.1\mathrm{PL}_{r,b,i}}$. For ease of expression, some denotations are defined as follows: $\hat{\mathbf{A}}_m=\sum_{i=1}^{L_{r,b}}\sum_{j=1}^{L_{m,r}}\mathrm{diag}\left(\hat{\mathbf{A}}_{m,r,j}\right)\hat{\mathbf{A}}_{r,b,i}^H\in\mathbb{C}^{N\times K}$, $\hat{\mathbf{A}}_{m,b}=\sum_{l=1}^{L_{m,b}}\hat{\mathbf{A}}_{m,b,l}\in\mathbb{C}^{K\times 1}$, $\mathrm{PL}_{m,r}=-10\log_{10}\left(\sum_{j=1}^{L_{m,r}}10^{-0.1\mathrm{PL}_{m,r,j}}\right)$, $\mathrm{PL}_{r,b}=-10\log_{10}\left(\sum_{i=1}^{L_{r,b}}10^{-0.1\mathrm{PL}_{r,b,i}}\right)$, and $\mathrm{PL}_{m,b}=-10\log_{10}\left(\sum_{l=1}^{L_{m,b}}10^{-0.1\mathrm{PL}_{m,b,l}}\right)$. Thus, $\mathbb{E}\left\{\left\|\rho_m\hat{\mathbf{h}}_m^H\boldsymbol{\theta}+\rho_{m,b}\hat{\mathbf{h}}_{m,b}\right\|^2\right\}$ can be formulated as

$$\begin{aligned}
&\mathbb{E}\left\{\left\|\rho_m\hat{\mathbf{h}}_m^H\boldsymbol{\theta}+\rho_{m,b}\hat{\mathbf{h}}_{m,b}\right\|^2\right\}\\
=&\varpi_m\left\|\hat{\mathbf{A}}_m^H\boldsymbol{\theta}\right\|^2 10^{-0.1(\mathrm{PL}_{m,r}+\mathrm{PL}_{r,b})}+\varpi_{m,b}\left\|\hat{\mathbf{A}}_{m,b}\right\|^2 10^{-0.1\mathrm{PL}_{m,b}}.
\end{aligned}\tag{36}$$

Next, the second term of (33), i.e., $\mathbb{E}\left\{\left\|\Delta\mathbf{h}_m^H\boldsymbol{\theta}+\Delta\mathbf{h}_{m,b}\right\|^2\right\}$, is analyzed as follows. Since both $\Delta\mathbf{h}_{m,b}$ and $\Delta\mathbf{h}_m$ follow complex Gaussian distribution with zero mean and they are independent of each other, we have

$$\begin{aligned}
&\mathbb{E}\left\{\left\|\Delta\mathbf{h}_m^H\boldsymbol{\theta}+\Delta\mathbf{h}_{m,b}\right\|^2\right\}=\mathbb{E}\left\{\left\|\Delta\mathbf{h}_m^H\boldsymbol{\theta}\right\|^2\right\}+\mathbb{E}\left\{\left\|\Delta\mathbf{h}_{m,b}\right\|^2\right\}\\
=&\mathbb{E}\left\{\mathrm{vec}^T\left(\Delta\mathbf{h}_m\right)\left(\mathbf{I}_K\otimes\boldsymbol{\Theta}\right)\mathrm{vec}\left(\Delta\mathbf{h}_m^*\right)\right\}+\mathbb{E}\left\{\Delta\mathbf{h}_{m,b}^H\Delta\mathbf{h}_{m,b}\right\}\\
=&\left(\eta_m^c\right)^2\left(1-\rho_m^2\right)\mathbb{E}\left\{\left(\mathbf{i}_m^c\right)^T\left(\mathbf{I}_K\otimes\boldsymbol{\Theta}\right)\left(\mathbf{i}_m^c\right)^*\right\}\\
&+\left(\eta_m^d\right)^2\left(1-\rho_{m,b}^2\right)\mathbb{E}\left\{\left(\mathbf{i}_m^d\right)^H\left(\mathbf{i}_m^d\right)\right\}\\
\overset{(a)}{=}&\left(\eta_m^c\sqrt{1-\rho_m^2}\right)^2\left(\mathrm{Tr}\left(\mathbf{I}_K\otimes\boldsymbol{\Theta}\right)+\mathbb{E}\left\{\left(\mathbf{i}_m^c\right)^T\right\}\left(\mathbf{I}_K\otimes\boldsymbol{\Theta}\right)\mathbb{E}\left\{\mathbf{i}_m^c\right\}\right)\\
&+\left(\eta_{m,b}^d\sqrt{1-\rho_{m,b}^2}\right)^2\left(\mathrm{Cov}\left(\mathbf{i}_m^c,\mathbf{i}_m^c\right)+\mathbf{i}_m^d\left(\mathbf{i}_m^d\right)^H\right)\\
=&\left(\left(\eta_m^c\sqrt{1-\rho_m^2}\right)^2+\left(\eta_m^d\sqrt{1-\rho_{m,b}^2}\right)^2\right)NK,
\end{aligned}\tag{37}$$

where (a) comes from [36, in P35]. By combining the results in (36) and (37), we obtain

$$\begin{aligned}
&\mathbb{E}\left\{\left\|\mathbf{h}_m^H\boldsymbol{\theta}+\mathbf{h}_{m,b}\right\|^2\right\}\\
=&\varpi_m\left\|\hat{\mathbf{A}}_m^H\boldsymbol{\theta}\right\|^2 10^{-0.1(\mathrm{PL}_{m,r}+\mathrm{PL}_{r,b})}+\varpi_{m,b}\left\|\hat{\mathbf{A}}_{m,b}\right\|^2 10^{-0.1\mathrm{PL}_{m,b}}\\
&+\left(\left(\eta_m^c\sqrt{1-\rho_m^2}\right)^2+\left(\eta_m^d\sqrt{1-\rho_{m,b}^2}\right)^2\right)NK,
\end{aligned}\tag{38}$$

and we thus complete the proof.

## Appendix B
## Proof of Proposition 2

The constraint (12b) is equivalent to $\Pr\left(P_m\left\|\mathbf{h}_m^H\boldsymbol{\theta}+\mathbf{h}_{m,b}\right\|^2\geq\sigma^2\gamma^{\mathrm{th}}\right)\geq 1-p_0,\forall m$, and the left hand side of this inequality can be reformulated as (39), shown at the top of the next page. The second term of (39), i.e., $2\Re\left\{\left(\rho_m\hat{\mathbf{h}}_m^H\boldsymbol{\theta}+\rho_{m,b}\hat{\mathbf{h}}_{m,b}\right)^H\left(\Delta\mathbf{h}_m^H\boldsymbol{\theta}+\Delta\mathbf{h}_{m,b}\right)\right\}$, can be written as (40) at the top of the next page, where

$$\begin{aligned}
&\Pr\left\{\left[\left(\rho_m\hat{\mathbf{h}}_m^H\boldsymbol{\theta}+\rho_{m,b}\hat{\mathbf{h}}_{m,b}\right)+\left(\Delta\mathbf{h}_m^H\boldsymbol{\theta}+\Delta\mathbf{h}_{m,b}\right)\right]^H\left[\left(\rho_m\hat{\mathbf{h}}_m^H\boldsymbol{\theta}+\rho_{m,b}\hat{\mathbf{h}}_{m,b}\right)+\left(\Delta\mathbf{h}_m^H\boldsymbol{\theta}+\Delta\mathbf{h}_{m,b}\right)\right]\geq\sigma^2\gamma^{\mathrm{th}}/P_m\right\}\\
=&\Pr\left\{\left(\rho_m\hat{\mathbf{h}}_m^H\boldsymbol{\theta}+\rho_{m,b}\hat{\mathbf{h}}_{m,b}\right)^H\left(\rho_m\hat{\mathbf{h}}_m^H\boldsymbol{\theta}+\rho_{m,b}\hat{\mathbf{h}}_{m,b}\right)+2\Re\left\{\left(\rho_m\hat{\mathbf{h}}_m^H\boldsymbol{\theta}+\rho_{m,b}\hat{\mathbf{h}}_{m,b}\right)^H\left(\Delta\mathbf{h}_m^H\boldsymbol{\theta}+\Delta\mathbf{h}_{m,b}\right)\right\}\right.\\
&\left.+\left(\Delta\mathbf{h}_m^H\boldsymbol{\theta}+\Delta\mathbf{h}_{m,b}\right)^H\left(\Delta\mathbf{h}_m^H\boldsymbol{\theta}+\Delta\mathbf{h}_{m,b}\right)\geq\sigma^2\gamma^{\mathrm{th}}/P_m\right\}. \qquad (39)
\end{aligned}$$

$$\begin{aligned}
&2\Re\left\{\mathrm{vec}^T\left(\boldsymbol{\theta}\left(\rho_m\boldsymbol{\theta}^H\hat{\mathbf{h}}_m+\rho_{m,b}\hat{\mathbf{h}}_{m,b}^H\right)\right)\mathrm{vec}\left(\Delta\mathbf{h}_m^*\right)+\left(\rho_m\boldsymbol{\theta}^H\hat{\mathbf{h}}_m+\rho_{m,b}\hat{\mathbf{h}}_{m,b}^H\right)\Delta\mathbf{h}_{m,b}\right\}\\
=&2\Re\left\{\eta_m^c\sqrt{1-\rho_m^2}\mathrm{vec}^T\left(\boldsymbol{\theta}\left(\boldsymbol{\theta}^H\rho_m\hat{\mathbf{h}}_m+\rho_{m,b}\hat{\mathbf{h}}_{m,b}^H\right)\right)\left(\mathbf{i}_m^c\right)^*+\eta_m^d\sqrt{1-\rho_{m,b}^2}\left(\boldsymbol{\theta}^H\rho_m\hat{\mathbf{h}}_m+\rho_{m,b}\hat{\mathbf{h}}_{m,b}^H\right)\mathbf{i}_m^d\right\}\\
\triangleq&2\Re\left\{\mathbf{v}_m^H\mathbf{i}_m\right\}. \qquad (40)
\end{aligned}$$

$$\boldsymbol{\Lambda}_m=\begin{bmatrix}\left(\eta_m^c\sqrt{1-\rho_m^2}\right)^2\left(\mathbf{I}_K\otimes\boldsymbol{\Theta}\right) & \eta_m^c\eta_m^d\sqrt{\left(1-\rho_m^2\right)\left(1-\rho_{m,b}^2\right)}\left(\mathbf{I}_K\otimes\boldsymbol{\theta}^*\right)\\ \eta_m^c\eta_m^d\sqrt{\left(1-\rho_m^2\right)\left(1-\rho_{m,b}^2\right)}\left(\mathbf{I}_K\otimes\boldsymbol{\theta}^T\right) & \left(\eta_m^d\sqrt{1-\rho_{m,b}^2}\right)^2\mathbf{I}_K\end{bmatrix}. \qquad (41)$$

$$\mathbf{v}_m=\begin{bmatrix}\eta_m^c\sqrt{1-\rho_m^2}\mathrm{vec}^*\left(\boldsymbol{\theta}\left(\rho_m\boldsymbol{\theta}^H\hat{\mathbf{h}}_m+\rho_{m,b}\hat{\mathbf{h}}_{m,b}^H\right)\right)\\ \eta_m^d\sqrt{1-\rho_{m,b}^2}\left(\rho_m\hat{\mathbf{h}}_m^H\boldsymbol{\theta}+\rho_{m,b}\hat{\mathbf{h}}_{m,b}\right)\end{bmatrix}$$

and $\mathbf{i}_m=\begin{bmatrix}\left(\mathbf{i}_m^c\right)^T & \left(\mathbf{i}_m^d\right)^H\end{bmatrix}^H$. The third term of (39), i.e., $\left(\Delta\mathbf{h}_m^H\boldsymbol{\theta}+\Delta\mathbf{h}_{m,b}\right)^H\left(\Delta\mathbf{h}_m^H\boldsymbol{\theta}+\Delta\mathbf{h}_{m,b}\right)$, can be organized as

$$\begin{aligned}
&\boldsymbol{\theta}^H\Delta\mathbf{h}_m\Delta\mathbf{h}_m^H\boldsymbol{\theta}+2\Re\left\{\boldsymbol{\theta}^H\Delta\mathbf{h}_m\Delta\mathbf{h}_{m,b}\right\}+\Delta\mathbf{h}_{m,b}^H\Delta\mathbf{h}_{m,b}\\
=&\mathrm{vec}^T\left(\Delta\mathbf{h}_m\right)\left(\mathbf{I}_K\otimes\boldsymbol{\Theta}\right)\mathrm{vec}\left(\Delta\mathbf{h}_m^*\right)\\
&+2\Re\left\{\Delta\mathbf{h}_{m,b}\left(\mathbf{I}_K\otimes\boldsymbol{\theta}^T\right)\mathrm{vec}\left(\Delta\mathbf{h}_m^*\right)\right\}+\Delta\mathbf{h}_{m,b}^H\Delta\mathbf{h}_{m,b}\\
=&\left(\eta_m^c\sqrt{1-\rho_m^2}\right)^2\left(\mathbf{i}_m^c\right)^T\left(\mathbf{I}_K\otimes\boldsymbol{\Theta}\right)\left(\mathbf{i}_m^c\right)^*\\
&+2\Re\left\{\eta_m^c\eta_m^d\sqrt{\left(1-\rho_m^2\right)\left(1-\rho_{m,b}^2\right)}\left(\mathbf{i}_m^d\right)^H\left(\mathbf{I}_K\otimes\boldsymbol{\theta}^T\right)\left(\mathbf{i}_m^c\right)^*\right\}\\
&+\left(\eta_m^d\sqrt{1-\rho_{m,b}^2}\right)^2\left(\mathbf{i}_m^d\right)^H\left(\mathbf{i}_m^d\right)\\
\triangleq&\mathbf{i}_m^H\boldsymbol{\Lambda}_m\mathbf{i}_m, \qquad (42)
\end{aligned}$$

where $\boldsymbol{\Lambda}_m$ is given by (41), shown at the top of this page. By combining the results in (40) and (42), we can obtain the expression in (13). Hence, the proof is completed.

## REFERENCES


[1] S. Zeadally, M. A. Javed, and E. B. Hamida, "Vehicular communications for ITS: Standardization and challenges," *IEEE Commun. Standards Mag.*, vol. 4, no. 1, pp. 11–17, Mar. 2020.

[2] T. Zugno, M. Drago, M. Giordani, M. Polese, and M. Zorzi, "Toward standardization of millimeter-wave vehicle-to-vehicle networks: Open challenges and performance evaluation," *IEEE Commun. Mag.*, vol. 58, no. 9, pp. 79–85, Sep. 2020.

[3] IEEE, "802.11 NGV proposed PAR," Study Group on 802.11bd (TGbd) 802.11-18/0861r8, Tech. Rep., May 2019.

[4] *Technical Specification Group Radio Access Network; Study on NR Vehicle-to-Everything (V2X) (Release 16)*, document 3GPP TR 38.885 V16.0.0, 3rd Generation Partnership Project, Mar. 2019.

[5] B. Coll-Perales, J. Gozalvez, and M. Gruteser, "Sub-6GHz assisted MAC for millimeter wave vehicular communications," *IEEE Commun. Mag.*, vol. 57, no. 3, pp. 125–131, Mar. 2019.

[6] M. Di Renzo, A. Zappone, M. Debbah, M. S. Alouini, C. Yuen, J. de Rosny, and S. Tretyakov, "Smart radio environments empowered by reconfigurable intelligent surfaces: How it works, state of research, and the road ahead," *IEEE J. Sel. Areas Commun.*, vol. 38, no. 11, pp. 2450–2525, Nov. 2020.

[7] J. Zhang, E. Björnson, M. Matthaiou, D. W. K. Ng, H. Yang, and D. J. Love, "Prospective multiple antenna technologies for beyond 5G," *IEEE J. Sel. Areas Commun.*, vol. 38, no. 8, pp. 1637–1660, Aug. 2020.

[8] Y. Chen, Y. Wang, J. Zhang, and Z. Li, "Resource allocation for intelligent reflecting surface aided vehicular communications," *IEEE Trans. Veh. Technol.*, vol. 69, no. 10, pp. 12 321–12 326, Oct. 2020.

[9] Y. Chen, Y. Wang, J. Zhang, and M. Di Renzo, "QoS-driven spectrum sharing for reconfigurable intelligent surfaces (RISs) aided vehicular networks," *IEEE Trans. Wireless Commun.*, to appear, 2021.

[10] A. Zappone, M. Di Renzo, F. Shams, X. Qian, and M. Debbah, "Overhead-aware design of reconfigurable intelligent surfaces in smart radio environments," *IEEE Trans. Wireless Commun.*, vol. 20, no. 1, pp. 126–141, Jan. 2021.

[11] L. Liang, H. Ye, and G. Y. Li, "Spectrum sharing in vehicular networks based on multi-agent reinforcement learning," *IEEE J. Sel. Areas Commun.*, vol. 37, no. 10, pp. 2282–2292, Oct. 2019.

[12] A. Abrardo, D. Dardari, and M. Di Renzo, "Intelligent reflecting surfaces: Sum-rate optimization based on statistical CSI," *arXiv preprint arXiv:2012.10679*, 2020.

[13] K. Zhi, C. Pan, H. Ren, and K. Wang, "Power scaling law analysis and phase shift optimization of RIS-aided massive MIMO systems with statistical CSI," *arXiv preprint arXiv:2010.13525*, 2020.

[14] M. Zhao, Q. Wu, M. J. Zhao, and R. Zhang, "Intelligent reflecting surface enhanced wireless network: Two-timescale beamforming optimization," *IEEE Trans. Wireless Commun.*, vol. 20, no. 1, pp. 2–17, Jan. 2021.

[15] M. Zhao, A. Liu, Y. Wan, and R. Zhang, "Two-timescale beamforming optimization for intelligent reflecting surface aided multiuser communication with QoS constraints," *IEEE Trans. Wireless Commun.*, to appear, 2021.

[16] X. Yu, D. Xu, Y. Sun, D. W. K. Ng, and R. Schober, "Robust and secure wireless communications via intelligent reflecting surfaces," *IEEE J. Sel. Areas Commun.*, vol. 38, no. 11, pp. 2637–2652, Nov. 2020.

[17] G. Zhou, C. Pan, H. Ren, K. Wang, and A. Nallanathan, "A framework of robust transmission design for IRS-aided MISO communications with imperfect cascaded channels," *IEEE Trans. Signal Process.*, vol. 68, pp. 5092–5106, Aug. 2020.

[18] G. Zhou, C. Pan, H. Ren, K. Wang, M. D. Renzo, and A. Nallanathan, "Robust beamforming design for intelligent reflecting surface aided MISO communication systems," *IEEE Wireless Commun. Lett.*, vol. 9, no. 10, pp. 1658–1662, Oct. 2020.

[19] T. A. Le, T. Van Chien, and M. D. Renzo, "Robust probabilistic-

constrained optimization for IRS-aided MISO communication systems," *IEEE Wireless Commun. Lett.*, vol. 10, no. 1, pp. 1–5, Jan. 2021.
[20] Z. Wang, L. Liu, and S. Cui, "Channel estimation for intelligent reflecting surface assisted multiuser communications: Framework, algorithms, and analysis," *IEEE Trans. Wireless Commun.*, vol. 19, no. 10, pp. 6607–6620, Oct. 2020.
[21] Q. Qin, L. Gui, P. Cheng, and B. Gong, "Time-varying channel estimation for millimeter wave multiuser MIMO systems," *IEEE Trans. Veh. Technol.*, vol. 67, no. 10, pp. 9435–9448, Oct. 2018.
[22] X. Xia, K. Xu, S. Zhao, and Y. Wang, "Learning the time-varying massive MIMO channels: Robust estimation and data-aided prediction," *IEEE Trans. Veh. Technol.*, vol. 69, no. 8, pp. 8080–8096, Aug. 2020.
[23] C. You, B. Zheng, and R. Zhang, "Channel estimation and passive beamforming for intelligent reflecting surface: Discrete phase shift and progressive refinement," *IEEE J. Sel. Areas Commun.*, vol. 38, no. 11, pp. 2604–2620, Nov. 2020.
[24] L. You, X. Gao, A. L. Swindlehurst, and W. Zhong, "Channel acquisition for massive MIMO-OFDM with adjustable phase shift pilots," *IEEE Trans. Signal Process.*, vol. 64, no. 6, pp. 1461–1476, Mar. 2016.
[25] M. Pätzold, *Mobile radio channels*. John Wiley & Sons, 2011.
[26] Y. Ma, D. Zhang, A. Leith, and Z. Wang, "Error performance of transmit beamforming with delayed and limited feedback," *IEEE Trans. Wireless Commun.*, vol. 8, no. 3, pp. 1164–1170, Mar. 2009.
[27] J. Zhang, M. Kountouris, J. G. Andrews, and R. W. Heath, "Multi-mode transmission for the MIMO broadcast channel with imperfect channel state information," *IEEE Trans. Commun.*, vol. 59, no. 3, pp. 803–814, Mar. 2011.
[28] A. Goldsmith, *Wireless communications*. Cambridge university press, 2005.
[29] K. Wang, A. M. So, T. Chang, W. Ma, and C. Chi, "Outage constrained robust transmit optimization for multiuser MISO downlinks: Tractable approximations by conic optimization," *IEEE Trans. Signal Process.*, vol. 62, no. 21, pp. 5690–5705, Nov. 2014.
[30] X. Zhang, *Matrix analysis and applications*. Cambridge University Press, 2017.
[31] M. Grant and S. Boyd, "CVX: Matlab software for disciplined convex programming, version 2.1," http://cvxr.com/cvx, Mar. 2014.
[32] T. Lipp and S. Boyd, "Variations and extension of the convex–concave procedure," *Optim. Eng.*, vol. 17, no. 2, pp. 263–287, Jun. 2016.
[33] M. ApS, "Mosek optimization toolbox for matlab, release 9.2.29," *User's Guide and Reference Manual,*, vol. 4, Oct. 2020.
[34] A. Ben-Tal and A. Nemirovski, *Lectures on modern convex optimization: analysis, algorithms, and engineering applications*. SIAM, 2001.
[35] A. Liu, V. K. N. Lau, and B. Kananian, "Stochastic successive convex approximation for non-convex constrained stochastic optimization," *IEEE Trans. Signal Process.*, vol. 67, no. 16, pp. 4189–4203, Aug. 2019.
[36] K. Petersen and M. Pedersen, "The matrix cookbook, version 20121115," *Technical Univ. Denmark, Kongens Lyngby, Denmark, Tech. Rep*, vol. 3274, Nov. 2012.
[37] *Technical Specification Group Radio Access Network; Study LTE-Based V2X Services; (Release 14)*, document 3GPP TR 36.885 V14.0.0, 3rd Generation Partnership Project, Jun. 2016.
[38] D. Zhao, H. Lu, Y. Wang, H. Sun, Y. Gui, and J. Wu, "Joint power allocation and user association optimization for IRS-assisted mmWave systems," *arXiv preprint arXiv:2010.11713*, 2020.
[39] O. E. Ayach, S. Rajagopal, S. Abu-Surra, Z. Pi, and R. W. Heath, "Spatially sparse precoding in millimeter wave MIMO systems," *IEEE Trans. Wireless Commun.*, vol. 13, no. 3, pp. 1499–1513, Mar. 2014.
[40] L. Dai, B. Wang, M. Wang, X. Yang, J. Tan, S. Bi, S. Xu, F. Yang, Z. Chen, M. D. Renzo, C. B. Chae, and L. Hanzo, "Reconfigurable intelligent surface-based wireless communications: Antenna design, prototyping, and experimental results," *IEEE Access*, vol. 8, pp. 45 913–45 923, Mar. 2020.
[41] X. Yang, Y. Liu, Y. Zhang, and Z. Yue, "Hybrid reliability analysis with both random and probability-box variables," *Acta Mech.*, vol. 226, no. 5, pp. 1341–1357, Dec. 2015.
[42] D. Berleant and C. Goodman-Strauss, "Bounding the results of arithmetic operations on random variables of unknown dependency using intervals," *Reliab. comput.*, vol. 4, no. 2, pp. 147–165, May 1998.
[43] M. K. Simon, *Probability distributions involving Gaussian random variables: A handbook for engineers and scientists*. Springer Science & Business Media, 2007.

**Yuanbin Chen** received the B.S. degree in communications engineering from the Beijing Jiaotong University, Beijing, China, in 2019. He is currently pursuing the Ph.D. degree in information and communication systems with the State Key Laboratory of Networking and Switching Technology, Beijing University of Posts and Telecommunications. His current research interests are in the area of reconfigurable intelligent surface (RIS), vehicle-to-everything (V2X), and radio resource management (RRM) in future wireless networks. He was the recipient of the National Scholarship in 2020.

**Ying Wang** received the Ph.D. degree in circuits and systems from the Beijing University of Posts and Telecommunications (BUPT), Beijing, China, in 2003. In 2004, she was invited to work as a Visiting Researcher with the Communications Research Laboratory (renamed NiCT from 2004), Yokosuka, Japan. She was a Research Associate with the University of Hong Kong, Hong Kong, in 2005. She is currently a Professor with BUPT and the Director of the Radio Resource Management Laboratory, Wireless Technology Innovation Institute, BUPT. Her research interests are in the area of the cooperative and cognitive systems, radio resource management, and mobility management in 5G systems. She is active in standardization activities of 3GPP and ITU. She took part in performance evaluation work of the Chinese Evaluation Group, as a Representative of BUPT. She was a recipient of first prizes of the Scientific and Technological Progress Award by the China Institute of Communications in 2006 and 2009, respectively, and a second prize of the National Scientific and Technological Progress Award in 2008. She was also selected in the New Star Program of Beijing Science and Technology Committee and the New Century Excellent Talents in University, Ministry of Education, in 2007 and 2009, respectively. She has authored over 100 papers in international journals and conferences proceedings.

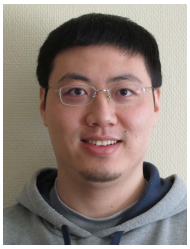

**Lei Jiao** (M'12-SM'18) received his BE degree from Hunan University, China, in 2005. He received his ME degree from Shandong University, China, in 2008. He obtained his PhD degree in Information and Communications Technology from University of Agder (UiA), Norway, in 2012. He is now an Associated Professor in the Department of Information and Communication Technology, UiA. His research interests include reinforcement learning, learning automata, natural language processing, resource allocation and performance evaluation for communication and energy systems.